CANADIAN THESES ON MICROFICHE

I.S.B.N.

THESES CANADIENNES SUR MICROFICHE

National Library of Canada
Collections Development Branch

Canadian Theses on
Microfiche Service

Ottawa, Canada
K1A 0N4

Bibliothèque nationale du Canada
Direction du développement des collections

Service des thèses canadiennes
sur microfiche

NOTICE

The quality of this microfiche is heavily dependent upon the quality of the original thesis submitted for microfilming. Every effort has been made to ensure the highest quality of reproduction possible.

If pages are missing, contact the university which granted the degree.

Some pages may have indistinct print especially if the original pages were typed with a poor typewriter ribbon or if the university sent us a poor photocopy.

Previously copyrighted materials (journal articles, published tests, etc.) are not filmed.

Reproduction in full or in part of this film is governed by the Canadian Copyright Act, R.S.C. 1970, c. C-30. Please read the authorization forms which accompany this thesis.

AVIS

La qualité de cette microfiche dépend grandement de la qualité de la thèse soumise au microfilmage. Nous avons tout fait pour assurer une qualité supérieure de reproduction.

S'il manque des pages, veuillez communiquer avec l'université qui a conféré le grade.

La qualité d'impression de certaines pages peut laisser à désirer, surtout si les pages originales ont été dactylographiées à l'aide d'un ruban usé ou si l'université nous a fait parvenir une photocopie de mauvaise qualité.

Les documents qui font déjà l'objet d'un droit d'auteur (articles de revue, examens publiés, etc.) ne sont pas microfilmés.

La reproduction, même partielle, de ce microfilm est soumise à la Loi canadienne sur le droit d'auteur, SRC 1970, c. C-30. Veuillez prendre connaissance des formules d'autorisation qui accompagnent cette thèse.

THIS DISSERTATION
HAS BEEN MICROFILMED
EXACTLY AS RECEIVED

LA THÈSE A ÉTÉ
MICROFILMÉE TELLE QUE
NOUS L'AVONS REÇUE

NL-339 (r. 82/08)

Canada

4/6

National Library of Canada | Bibliothèque nationale du Canada

CANADIAN THESES ON MICROFICHE | THÈSES CANADIENNES SUR MICROFICHE

62341

NAME OF AUTHOR/*NOM DE L'AUTEUR* Kenneth David Myrtle

TITLE OF THESIS/*TITRE DE LA THÈSE* The Temperature Dependence of the Transmission of 24 GHZ radiation through Electrolytically formed Nickel Single Crystals

UNIVERSITY/*UNIVERSITÉ* Simon Fraser University

DEGREE FOR WHICH THESIS WAS PRESENTED/*GRADE POUR LEQUEL CETTE THÈSE FUT PRÉSENTÉE* M.Sc.

YEAR THIS DEGREE CONFERRED/*ANNÉE D'OBTENTION DE CE DEGRÉ* 1983

NAME OF SUPERVISOR/*NOM DU DIRECTEUR DE THÈSE* Professor John F. Cochran

Permission is hereby granted to the NATIONAL LIBRARY OF CANADA to microfilm this thesis and to lend or sell copies of the film.

The author reserves other publication rights, and neither the thesis nor extensive extracts from it may be printed or otherwise reproduced without the author's written permission.

L'autorisation est, par la présente, accordée à la BIBLIOTHÈQUE NATIONALE DU CANADA de microfilmer cette thèse et de prêter ou de vendre des exemplaires du film.

L'auteur se réserve les autres droits de publication; ni la thèse ni de longs extraits de celle-ci ne doivent être imprimés ou autrement reproduits sans l'autorisation écrite de l'auteur.

DATED/*DATE* 19/APRIL/83 SIGNED/*SIGNÉ* [redacted]

PERMANENT ADDRESS/*RÉSIDENCE FIXE* [redacted]

CIHM (11-79)

THE TEMPERATURE DEPENDENCE OF THE TRANSMISSION OF 24 GHZ RADIATION THROUGH ELECTROLYTICALLY FORMED NICKEL SINGLE CRYSTALS

by

Kenneth David Myrtle

B.Sc., Simon Fraser University, 1979

A THESIS SUBMITTED IN PARTIAL FULFILLMENT OF

THE REQUIREMENTS FOR THE DEGREE OF

MASTER OF SCIENCE

in the Department

of

Physics

SIMON FRASER UNIVERSITY

April 1983

PARTIAL COPYRIGHT LICENSE

I hereby grant to Simon Fraser University the right to lend my thesis, project or extended essay (the title of which is shown below) to users of the Simon Fraser University Library, and to make partial or single copies only for such users or in response to a request from the library of any other university, or other educational institution, on its own behalf or for one of its users. I further agree that permission for multiple copying of this work for scholarly purposes may be granted by me or the Dean of Graduate Studies. It is understood that copying or publication of this work for financial gain shall not be allowed without my written permission.

Title of Thesis/Project/Extended Essay

The Temperature Dependence of the Transmission of 24 GHZ radiation through Electrolytically formed Nickel Single Crystals

Author:

(signature)

Kenneth David MYRTLE

(name)

19 APRIL 1983

(date)

APPROVAL

Name: Kenneth David Myrtle

Degree: Master of Science

Title of Thesis: The temperature dependence of the transmission of 24 Ghz radiation through electrolytically formed nickel single crystals

Examining committee:

Chairman: B. P. Clayman

J. F. Cochran
Senior Supervisor

A. S. Arrott

B. Heinrich

R. H. Enns
External Examiner
Professor
Department of Physics
Simon Fraser University

Date Approved: April 8 1983

ABSTRACT

The transmission of 24 GHz radiation through nickel specimens has been measured over the temperature range 4 to 300 K using nickel single crystals which had been grown electrolytically on a copper single crystal substrate. The experimental results have been compared with a calculation which includes magneto-elastic coupling between the lattice and the magnetization. In general the theory gives a good account of the observed lineshapes and amplitudes. An estimate of the ultrasonic mean free path was made and the temperature dependence of the magnetic damping parameter corresponding to excitations having small wavenumbers was found to be in agreement with earlier results obtained on nickel crystals cut from the bulk by Heinrich Meredith and Cochran [1].

ACKNOWLEDGEMENTS

I would like to thank John Cochran for all of the assistance that he has given me during my years at SFU. I would also like to thank Bretislav Heinrich who was always willing to provide advice and assistance, and with whom I have spent many enjoyable hours working in the lab. I would also like to acknowledge the assistance provided the staff of the Machine Shop and the Department of Physics.

TABLE OF CONTENTS

LIST OF TABLES

LIST OF FIGURES

I. INTRODUCTION

The measurement of the response of a ferromagnetic material to a time varying magnetic field has proven to be a valuable technique for the study of its magnetic properties. This technique is particularly well suited to the study of the processes which allow the magnetization to relax back to an equilibrium state. Bhagat and coworkers [2,3,4] have made measurements of the magnetic relaxation parameter in iron, cobalt, and nickel at microwave frequencies by measuring the power absorption at ferromagnetic resonance (FMR) and found that nickel exhibited a large increase in the magnetic damping at low temperatures. Measurements on copper-nickel alloys [4] seemed to suggest that the increase in magnetic damping was related to the rise in the electrical conductivity at low temperatures. Kambersky [5] and Prange and Korenmann [6] have proposed a theoretical explanation for the observed increase in magnetic damping at low temperatures. This theory predicts that the magnetic damping would become both wavenumber and frequency dependent when the electrical conductivity becomes non-local. By non-local we mean that the electron mean free path is comparable to or longer than the wavelength of the disturbance. A consequence of the long mean free path is that ohms law which relates the current density at a point to the local electric field is no longer valid. In metals FMR measurements excite the material at relatively large wave numbers (10^5 cm^{-1} at 24 GHz) and so the conductivity begins to become non-local at temperatures as high as 150 K.

In order to test this theory it was necessary to measure the magnetic damping as a function of frequency or wavenumber. Heinrich, Meredith and Cochran [1] measured the magnetic damping in nickel at very small

wavenumbers using the technique of microwave transmission at ferromagnetic antiresonance (FMAR). These measurements were made in the temperature range from 90-300 K. The present work was motivated by a desire to extend their measurements to lower temperatures. In particular, we had hoped to be able to test the formula for the wavenumber dependent magnetic damping in nickel reported by Heinrich, Meredith and Cochran [1].

In order to help acquaint the reader with the techniques which are used to measure magnetic damping a brief outline of the equations which describe the response of a ferromagnet to a time varying magnetic field follows. For simplicity torques due to magnetocrystalline anisotropy, magnetostriction and exchange have been neglected. These will be discussed in Chapter 2 "Theory".

Although we will describe the motion of the sample magnetization in classical terms it should be noted that the forces which maintain the sample in a ferromagnetic state are of a quantum mechanical nature (the very large quantum numbers associated with the sample magnetization suggest that a classical treatment is justified).

Associated with the magnetic moment of the sample $\bar{M}$ there is an angular momentum $\bar{L}$ and they are related by the magnetomechanical ratio γ

$$\bar{M} = -\gamma \bar{L} \qquad 1.1$$

In most magnetic materials γ has a value that is close to that which would be expected for a free electron and so we define

$$\gamma = \frac{g|e|}{2mc} \qquad 1.2$$

with the g factor taking on different values in different materials (g = 2.0023 for a free electron, g = 2.18 for nickel etc.). If we apply a magnetic field $\bar{H}$ to the sample the magnetization will experience a torque

equal to

$$1.3 \qquad \bar{\tau} = \bar{M} \times \bar{H}$$

which leads to

$$1.4 \qquad \frac{d\bar{M}}{dt} = -\gamma (\bar{M} \times \bar{H})$$

We have now arrived at an equation of motion for the magnetization in the absence of any damping. A phenomenological damping term can be included in this equation. Using the Gilbert form of damping [7] we have

$$1.5 \qquad \frac{d\bar{M}}{dt} = -\gamma (\bar{M} \times \bar{H}) - \frac{G}{\gamma M_s^2} (\bar{M} \times \bar{M})$$

In the experimental arrangement which we have used a thin slab of the material to be studied was mounted so as to form part of the end wall of a microwave cavity. A large D.C. magnetic field was then applied in the plane of the sample with the D.C. field oriented so as to be perpendicular to the microwave magnetic field at the surface of the sample. Under these circumstances and in the approximation that the time varying fields were small compared with the D.C. field and that the D.C. field was large enough to saturate the sample, equation 1.5 yields an R.F. permeability

$$1.6 \qquad \mu = \frac{B^2 - \omega^2/\gamma^2 - 2iB(\omega/\gamma)(G/\gamma M_s)}{BH - \omega^2/\gamma^2 - i(B+H)(\omega/\gamma)(G/\gamma M_s)}$$

where $\bar{B} = \bar{H} + 4\pi\bar{M}_s$ and ω is the applied microwave frequency. By inspection of equation 1.6 we can see that the permeability μ takes on a maximum value at $\sqrt{BH} = \omega/\gamma$. At this value of applied field the natural precessional frequency of the magnetization is equal to that of the applied microwave signal. This condition is known as ferromagnetic resonance (FMR). The amount of power absorbed by the sample reaches a maximum at

FMR and this results in a lowering of the Q of the microwave cavity. Hence by monitoring the Q of the cavity one can determine the FMR linewidth which can in turn be used to determine the value of the Gilbert damping parameter G. Although it is experimentally quite easy to measure the FMR linewidth this technique suffers from a number of shortcomings.

1./ Because of the large permeability at FMR the skin depth $\delta = (c^2/4\pi\omega\sigma'\mu)^{1/2}$ is very short typically 1000 Å in nickel at room temperature and at 24 GHz. Consequently, measurements made at FMR are very sensitive to the surface quality of the specimen.

2./ Even at moderately low temperatures (77 K) the electron mean free path begins to exceed the classical skin depth and effects due to non-local conductivity must be taken into account.

3./ A short skin depth implies rapid spatial variations in the direction of the magnetization. These spatial variations are resisted by the exchange field, the field which tends to maintain the parallel spin arrangement in a ferromagnet. The presence of the exchange field can result in a considerable increase in the FMR linewidth and consequently it must be taken into account before G can be determined. (This effect is large for iron, but relatively unimportant for nickel. In nickel the correction to the linewidth at 24 GHz is approximately 20 percent).

4./ The applied microwave field causes the sample magnetization to precess in a mode which has a spatial variation in the z direction only. The presence of inhomogeneities in the sample can cause energy to be lost to spatially non-uniform precessional modes (spin waves) by a process known as two magnon scattering (see Marshall Sparks for a detailed discussion of two magnon scattering [8]). At fields near FMR the mode excited by the microwave field is energetically degenerate with spin waves having small wavenumbers. The result is that measurements made at FMR are strongly

affected by sample inhomogeneities.

For all of these reasons one would prefer to have an alternative method for measuring G. Inspection of Equation 1.6 suggests a second method for measuring G. At a field $B_{INT} = \omega/\gamma$ the permeability, μ, takes on a minimum value, and this minimum value is determined by G. The small value of μ at ferromagnetic antiresonance (FMAR) implies that the skin depth will be much greater than that which would be observed in a normal metal having the same conductivity. The amount of radiation transmitted through a metal slab depends exponentially on the ratio of the thickness to the skin depth; therefore the amount of power transmitted at FMAR will be greatly enhanced over the power transmitted by a non-magnetic specimen of the same conductivity. The usefulness of FMAR transmission measurements for determining the magnetic properties of ferromagnetic metals was first demonstrated by Heinrich and Meshcharyakov [9,10]. Their method is free from the problems (1-3 above) which occurred at FMR as a result of the short skin depth. In addition, at FMAR the energetically degenerate spinwaves lie at much higher wavevectors than the uniform mode. This seems to greatly reduce the sensitivity of FMAR measurements to sample inhomogeneities. Unfortunately some new experimental difficulties arise. First the sample must be uniform in thickness so that the effective skin depth, and hence G, can be accurately determined. Also the sample must be thin enough that an observable amount of microwave radiation is transmitted at FMAR (a minimum of 10^{-17} watts can be detected).

In order to see a signal at FMAR through nickel at room temperature the sample thickness must be less than 20 μm. However as it was our intention to measure G down to 77 K where both the electrical conductivity

and the magnetic damping (G) have increased it became necessary to use nickel crystals only 2-3 μm thick. Pure nickel at 77 K has a conductivity which is approximately 14 times larger than the room temperature value and the magnetic damping is expected to be about 6 times larger than the room temperature value [1]. Hence the ratio of the sample thickness to the skin depth will have increased by a factor of approximately $9 \approx (14 \cdot 6)^{.5}$. And so a 2 μm thick sample at 77 K will have approximately the same size FMAR transmission signal as an 18 μm sample at room temperature. It should be noted that the use of such thin crystals results in a rather weak dependence of the transmitted signal on G at room temperature (at FMAR the signal basically travels across the sample unattenuated).

The production of such thin single crystals from the bulk presents the major obstacle to the measurement of G at low temperatures by the FMAR transmission technique. A number of attempts at producing uniformly thin crystals from bulk nickel crystals by mechanical and electrochemical polishing were made with little success. As a result of these difficulties a new method of sample preparation was sought. Nickel crystals can be grown epitaxially on a suitable copper substrate by electrolytic deposition [11]. Using this technique (described in detail in chapter 3) we were able to grow crystals which were both thin and uniform in thickness. It would appear that one should be able to use such epitaxially grown nickel single crystals to obtain G as a function of temperature from a straightforward measurement of FMAR transmission signals. However another problem arose. A large transmission signal was observed in the epitaxially grown crystals at the field corresponding to FMR. This signal was due to power transmitted across the sample by an ultrasonic wave. The FMR transmission signal is generated as a result of the magnetostrictive

coupling between the lattice and the precessing magnetization. At low temperatures this phonon signal became very large compared with the FMAR signal, and as a result the lowest temperature at which G could be measured was not limited by the ultimate sensitivity of the apparatus but rather by the condition that the FMAR signal be readily distinguished from the ultrasonic signal. It should be noted that Heinrich, Meredith and Cochran did not encounter this problem because their sample was not sufficiently plane parallel for the ultrasonic signal to arrive at the rear surface with a well defined phase.

In spite of the interference from the ultrasonic signal it was possible to confirm the results obtained by Heinrich et al. In addition, these are the first measurements for which the calculated and observed transmission signal amplitudes at FMR were in agreement. In all previous measurements the observed amplitude was at least 10 times smaller than was expected [12]. This was probably due to interference effects which one would expect to result from a non-uniform sample thickness. The ultrasonic attenuation length was found to be independent of temperature within experimental error.

Outline of thesis

Directly following this introduction is an outline of the equations of motion for the magnetization and lattice when terms due to anisotropy, exchange and magnetostriction are included. The equations of motion are then combined with Maxwell's equations in order to calculate the response of the sample to the incident microwave radiation. The second portion of this chapter contains a series of calculated curves which illustrate the dependence of the transmitted signal amplitude on the various parameters which are used in the theory. Chapter 3 contains a detailed description of how the epitaxial single crystal samples were made. This is followed by a description of the microwave measurements. Chapter 4 contains the results of the fitting of the experimental data to the theory outlined in Chapter 2. The discussion of these results is contained in Chapter 5.

II. THEORY

In this chapter we will be concerned with determining the amount of microwave radiation reflected from and transmitted through a thin slab of metal. In order to do this we need to know the equations of motion for the lattice and for the sample magnetization when terms due to magnetocrystalline anisotropy, magnetostriction and exchange have been included. We will start with the relationship between the magnetic moment per unit volume $\bar{M}$ and the angular momentum per unit volume $\bar{L}$.

$$\gamma \bar{L} = -\bar{M} \tag{2.1}$$

Which leads to

$$\frac{d\bar{M}}{dt} = -\gamma \bar{\tau} \tag{2.2}$$

where $\bar{\tau}$ is the net torque per unit volume acting on the magnetization. Before proceeding to describe the various torques which act on the magnetization a description of the particular geometry with which we will be dealing is required.

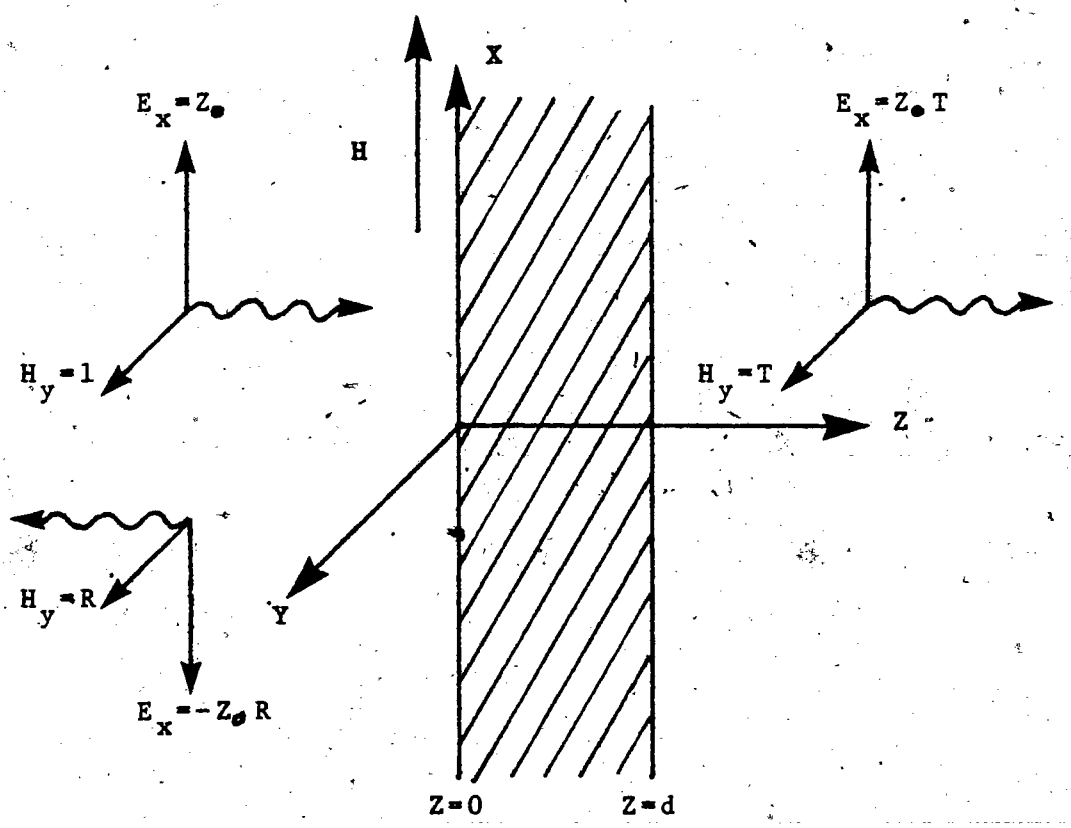

Fig. 2.1 A sketch of the sample geometry used in the calculations is shown above.

The sample is located between the two planes Z=0 and Z=d (see Fig. 2.1). A large external D.C. magnetic field is applied along the X axis and a small amplitude microwave frequency magnetic field is applied along the Y axis at Z=0. Under these conditions the magnetization will almost lie parallel to the X axis. We can write $\bar{M}=(M_s,m_y,m_z)$ since M_x will only differ from M_s by terms which are of second order in m_y and m_z. The first contribution to the net torque arises from the external fields and has the form

$$\bar{\tau}_H = \bar{M} \times \bar{H} \tag{2.3}$$

where $\bar{H}=(H_o,h_y,h_z)$ with H_o equal to the applied D.C. magnetic field (apart from static demagnetizing effects) and h_y and h_z are small microwave frequency magnetic fields.

At this point it is appropriate to make an allowance for the demagnetizing field produced by the sample magnetization. The magnetic field within the sample is less than the applied D.C. field by an amount $4\pi D_x M_x \doteq 4\pi D_x M_s$ where D_x is the demagnetizing factor in the X direction. The demagnetizing factor depends only on the sample geometry. For the infinite slab shown in Fig. 2.1 $D_x=0$. For a sample of finite size D_x will take on a non zero value. The demagnetizing factors are independent of position within the sample only for ellipsoidal shaped samples [13]. Fortunately the demagnetizing field for the very thin samples which we used was quite small and with sufficient accuracy (± 1 Oe) it could be assumed to be constant over the central region of the sample on which the measurements were made. Kraus and Frait [14] give an empirical expression for the demagnetizing field at the center of a disk (the applied field H_o is in the plane of the disk)

2.4 $$H_D = 2\pi M_s R\left(\{1+4R\}^{\frac{1}{2}} + .366\, M_s/H_o\right) = 4\pi M_s D_x$$

where R is the ratio of the thickness of the disk to its diameter. Typically for our samples $R=10^{-3}$, $2\pi M_s=3.2$ KOe and $M_s/H_o<.3$ so the demagnetizing field will be less than 4 Oe. The net effect is that we should use the internal field $H=(H_o-4\pi D_x M_s, h_y, h_z)$ rather than the external field in Equation 2.3.

A contribution to the torque on the magnetization arises from the phenomenological damping term. Using the form for the damping proposed by Gilbert in 1955 we have

2.5 $$\bar{\tau}_{damp} = \frac{-G}{(\gamma M_s)^2}\left(\bar{M} \times \frac{d\bar{M}}{dt}\right)$$

where G is a phenomenological damping parameter. This term introduces a torque proportional to the rate of change of $\bar{M}$ and so it looks like a viscous damping on the motion of $\bar{M}$. We have now included all of the terms which were introduced in the first chapter: we will now proceed to add those contributions to the torque which had been neglected in chapter one for the sake of simplicity.

The Exchange Field

The exchange field is a manifestation of the tendency for the magnetization to assume a parallel spin arrangement. If we expand the exchange energy density in terms of the components of $\bar{M}$ and their spatial derivatives keeping only those terms which contribute to the maintenance of a parallel spin arrangement and which satisfy the requirements for cubic symmetry we find that the lowest order term has the form [13]

2.6 $$E = \frac{A}{M_s^2}\left((\nabla M_x)^2 + (\nabla M_y)^2 + (\nabla M_z)^2\right)$$

where A is the exchange stiffness parameter. For the sample magnetization near the X axis and for spatial variations along the Z axis only (the signals are assumed to propagate along the Z axis as plane waves) we find that to first order in m_y and m_z the exchange energy produces a restoring torque on the magnetization of the form

$$2.7 \qquad \bar{\tau}_{ex} = \left(0, -M_s\left(\frac{2A}{M_s^2}\frac{\partial^2 M_z}{\partial Z^2}\right), M_s\left(\frac{2A}{M_s^2}\frac{\partial^2 M_y}{\partial Z^2}\right)\right)$$

If we write the torque in the form

$$2.8 \qquad \bar{\tau}_{ex} = \bar{M} \times \bar{H}_{ex}$$

Then to first order in m_y, m_z, h_y and h_z we have

$$2.9 \qquad \bar{H}_{ex} = \left(0, \frac{2A}{M_s^2}\frac{\partial^2 M_y}{\partial Z^2}, \frac{2A}{M^2}\frac{\partial^2 M_z}{\partial Z^2}\right).$$

Anisotropy

The next torque which we will consider arises from terms in the energy of the sample magnetization which depend upon the direction of the magnetization with respect to the crystallographic axis. Expanding the energy density, and keeping only those terms which are consistent with the cubic symmetry of the sample we find

$$2.10 \qquad E = K_1(\alpha_1^2\alpha_2^2 + \alpha_2^2\alpha_3^2 + \alpha_3^2\alpha_1^2) + K_2(\alpha_1^2\alpha_2^2\alpha_3^2)$$

where α_1, α_2 and α_3 are the direction cosines of the magnetization with respect to the three cube edges and where K_1 and K_2 are anisotropy constants. For almost all of the experimental measurements the applied field was parallel to the [100] crystal axis; under these conditions

$\alpha_1 = \frac{M_x}{M_s} \approx 1$ and $\alpha_2 \alpha_3 << 1$. The anisotropy energy then simplifies to

2.11 $$E = K_1 (\alpha_2^2 + \alpha_3^2)$$

which results in a torque on the magnetization of

2.12 $$\bar{\tau}_{AN} = \frac{2K_1}{M_s} (0, M_z, -M_y)$$

which can be written in the form

2.13 $$\bar{\tau}_{AN} = \bar{M} \times \bar{H}_{AN} \quad \text{where} \quad \bar{H}_{AN} = \left(\frac{2K_1}{M_s}, 0, 0\right)$$

It should be noted that the sample will not be saturated if the external field is not strong enough to overcome the effective anisotropy fields. In Nickel at low temperatures K_1 is less than zero and so we must apply a field larger than $|H_{an}|$ to saturate the magnetization and cause it to lie along the [100] direction. As our theory is only valid for saturated samples, the minimum field required to saturate the sample ($H=|2K_1/M_s|$) will be shown on all of the calculated curves.

Magnetostriction

The last torque which we shall consider is a result of the magnetoelastic coupling between the lattice and the magnetization. For a cubic crystal the total elastic and magnetoelastic energy density has the form [13]

2.14 $$\begin{aligned} E = {} & \tfrac{1}{2} C_{11} (\epsilon_{xx}^2 + \epsilon_{yy}^2 + \epsilon_{zz}^2) + \tfrac{1}{2} C_{44} (\epsilon_{xy}^2 + \epsilon_{yz}^2 + \epsilon_{zx}^2) + \\ & C_{12} (\epsilon_{xx}\epsilon_{yy} + \epsilon_{yy}\epsilon_{zz} + \epsilon_{zz}\epsilon_{xx}) + \\ & B_1 (\epsilon_{xx}(\alpha_1^2 - \tfrac{1}{3}) + \epsilon_{yy}(\alpha_2^2 - \tfrac{1}{3}) + \epsilon_{zz}(\alpha_3^2 - \tfrac{1}{3})) + \\ & B_2 (\alpha_1\alpha_2 \epsilon_{xy} + \alpha_2\alpha_3 \epsilon_{yz} + \alpha_3\alpha_1 \epsilon_{zx}) \end{aligned}$$

where

$$2.15 \qquad \epsilon_{xx} = \frac{\partial u}{\partial x} \;,\; \epsilon_{yy} = \frac{\partial v}{\partial y} \;,\; \epsilon_{zz} = \frac{\partial w}{\partial z}$$

$$2.16 \qquad \epsilon_{xy} = \frac{\partial u}{\partial y} + \frac{\partial v}{\partial x} \;,\; \epsilon_{yz} = \frac{\partial v}{\partial z} + \frac{\partial w}{\partial y} \;,\; \epsilon_{zx} = \frac{\partial w}{\partial x} + \frac{\partial u}{\partial z}$$

and B_1 and B_2 are the magnetostrictive coupling constants between the strains and the direction cosines of the magnetization. Again we will consider the case for which the applied D.C. field is along the [100] axis. By differentiating the energy with respect to the direction cosines of the magnetization we can determine the torques acting on the magnetization. To first order in α and ϵ we have a torque on the magnetization of $\tau_{ME} = (0, B_2\epsilon_{zx}, -B_2\epsilon_{xy})$ which reduces to

$$2.17 \qquad \tau_{ME} = \left(0, B_2 \frac{\partial u}{\partial z}, 0\right)$$

Since we will only be considering plane waves propagating in the Z direction. (This result is independent of the direction of propagation if the Z axis lies in the (100) plane.) It should be noted that if the sample is mechanically strained there will be additional terms in equation 2.17. For example J.R. Macdonald [15] has shown that if there is a uniform tension T in the (001) plane of the sample as a result of differential thermal contraction between the sample and the diaphragm on which it was mounted then Equation 2.17 will become

$$2.18 \qquad \tau_{ME} = \left(0, B_2 \frac{\partial u}{\partial z}, 0\right) + \frac{3\lambda_{100} T}{M_s} (0, M_2, 0)$$

where

2.19 $$\lambda_{100} = -\frac{2}{3}\frac{B_1}{(C_{11}-C_{12})}$$

These tension related effects can easily produce shifts of 100 Oe in the resonant fields.

This completes the list of torques acting on the magnetization. The equation of motion for the magnetization can be written as

2.20 $$\frac{\partial \bar{M}}{\partial t} = -\gamma\left(\bar{M}\times\bar{H}_{EFF} + \frac{G}{(\gamma M_s)^2}\left(\frac{\partial \bar{M}}{\partial t}\times\bar{M}\right) + \bar{\tau}_{ME}\right)$$

where 2.21 $$\bar{H}_{EFF} = \bar{H} + \bar{H}_{ex} + \bar{H}_{AN}$$

Before we can solve for the transmitted and reflected microwave signals we still need the equation of motion for the lattice. The forces acting on the lattice can be determined by differentiating the energy density with respect to the strains. For the geometry which we have been considering only a shear wave propagating in the Z direction with the displacement parallel to the X axis is excited. If we include a damping term for the lattice motion proportional to the velocity of the lattice, the magnetization is parallel to the [100] direction and the direction of propagation is along [100] or [110] we have

2.22 $$C_{44}\frac{\partial^2 u}{\partial z^2} + \frac{B_2}{M_s}\frac{\partial M_z}{\partial z} - \frac{\rho}{\tau}\frac{\partial u}{\partial t} = \rho\frac{\partial^2 u}{\partial t^2}$$

As all of the time dependent quantities vary as $e^{-kz+i\omega t}$ we find that to first order in the small quantities m_y, m_z, h_y and h_z Equation 2.20 becomes

2.23 $$-\frac{i\omega}{\gamma}M_y = \left(H_0 - 4\pi D_x M_s + \frac{2K_1}{M_s} - \frac{2Ak^2}{M_s} + \frac{i\omega G}{\gamma M_s}\right)M_z - B_2 k u - M_s h_z$$

2.24 $$\frac{i\omega}{\gamma}M_z = \left(H_0 - 4\pi D_x M_s + \frac{2K_1}{M_s} - \frac{2Ak^2}{M_s} + \frac{i\omega G}{\gamma M_s}\right)M_y - M_s h_y$$

These two equations are the linearized equations of motion for the sample magnetization.

In order to proceed further we must now combine the equations of motion for the lattice and sample magnetization with Maxwell's equations. In CGS units Maxwell's equations have the form

$$2.25 \quad \nabla \cdot \bar{D} = 4\pi\rho \qquad 2.26 \quad \nabla \times \bar{H} = \frac{4\pi}{c}\bar{J} + \frac{1}{c}\frac{\partial \bar{D}}{\partial t}$$

$$2.27 \quad \nabla \cdot \bar{B} = 0 \qquad 2.28 \quad \nabla \times \bar{E} = -\frac{1}{c}\frac{\partial \bar{B}}{\partial t}$$

We will assume that we have an isotropic dielectric constant ϵ and a scalar local conductivity ie. $\bar{J} = \sigma \bar{E}$. With these assumptions Maxwell's equations for plane waves propagating like $e^{-ikz+i\omega t}$, become

$$2.29 \quad -k\epsilon E_z = 4\pi\rho \qquad 2.30 \quad (kH_y, -kH_x, 0) = \left(\frac{4\pi\sigma}{c}, \frac{i\omega\epsilon}{c}\right)\bar{E}$$

$$2.31 \quad B_z = 0 \qquad 2.32 \quad (kE_y, -kE_x, 0) = -\frac{i\omega}{c}\bar{B}$$

from which $E_z=0$, $B_z=0=H_z+4\pi M_z$ and

$$2.33 \quad k^2 \begin{Bmatrix} H_x \\ H_y \end{Bmatrix} = \left(\frac{4\pi i\omega\sigma - \omega^2\epsilon}{c^2}\right) \begin{Bmatrix} B_x \\ B_y \end{Bmatrix}$$

In a metal such as Nickel the conduction current is much larger than the displacement current and so Equation 2.33 reduces to

$$2.34 \quad k^2 \begin{Bmatrix} H_x \\ H_y \end{Bmatrix} = \frac{i}{\delta^2} \begin{Bmatrix} B_x \\ B_y \end{Bmatrix}$$

where $\delta^2 = (c^2/4\pi\sigma\omega)$ is the classical skin depth. We are now in a position to eliminate the fields h_y and h_z from Equations 2.22 and 2.23. After having done that we find

$$2.35 \quad -\frac{i\omega}{\gamma} M_y = \left(H_0 - 4\pi M_s D_x + \frac{2k_1}{M_s} + 4\pi M_s - \frac{2Ak^2}{M_s} + \frac{i\omega G}{\gamma^2 M_s}\right) M_z - B_z K u$$

$$2.36 \quad \frac{i\omega}{\gamma} M_z = \left(H_0 - 4\pi M_s D_x + \frac{2k_1}{M_s} + \frac{4\pi M_s}{(1+\lambda k^2 \delta^2)} - \frac{2Ak^2}{M_s} + \frac{i\omega G}{\gamma^2 M_s}\right) M_y$$

By combining these two equations with the equation of motion for the lattice (2.21) we obtain the dispersion relation

$$2.37 \quad \frac{\omega^2}{\gamma^2} = \left(H_0 - 4\pi D_x M_s + \frac{2k_1}{M_s} - \frac{2Ak^2}{M_s} + \frac{i\omega G}{\gamma^2 M_s} + \frac{4\pi M_s}{(1+\lambda k^2 \delta^2)}\right) \times$$

$$\left(H_0 - 4\pi D_x M_s + \frac{2k_1}{M_s} - \frac{2Ak^2}{M_s} + \frac{i\omega G}{\gamma^2 M_s} + 4\pi M_s - \frac{B_z^2 k^2}{M_s (k^2 C_{44} + \rho\omega^2 - \frac{i\omega}{\tau}\rho)}\right)$$

This equation yields 4 eigenvalues for K^2. One corresponds to a mainly ultrasonic wave and the remaining three are coupled electromagnetic and spin waves.

We now have the solution for signal propagation within the sample. The amplitudes of the 8 waves within the sample and the amplitudes of the transmitted and reflected waves must be determined by matching boundary conditions at the front and rear surfaces. As there are 10 wave amplitudes to be determined we need 5 boundary conditions on each surface. Two boundary conditions at each surface arise straightforwardly from the conditions that the tangential components of e_x and h_y must be continuous across each surface.

It should be noted that our experiments were carried out in tuned microwave cavities and so the ratio of e_x to h_y at the surface of the sample will be different from the free space value of $Z_o = e_x / h_y = 1$. Although the transmitted signal amplitude is strongly dependent on the impedance Z the calculated lineshape is almost independent of the impedance

[16]. By mounting the sample between two tuned cavities (each with a cavity quality factor of Q) the observed signal amplitude is increased by a factor of approximately Q over the amplitude which would be observed if the sample was simply placed across the waveguide.

The total force acting on the lattice at the surface yields a third pair of boundary conditions, one at each surface. If the surface is free of any surface mass (ie. a thick oxide layer) the acoustic boundary conditions are

$$2.38 \qquad C_{44} \frac{\partial u}{\partial z}\Big|_{z=0,d} + \frac{B_2}{M_s} M_z\Big|_{z=0,d} = 0$$

The remaining two boundary conditions are a result of summing the surface torques acting on the magnetization, these boundary conditions were first described by Rado and Weertman in 1959 [17]. The particular boundary conditions which we have used are

$$2.39 \qquad A \frac{\partial M_y}{\partial z}\Big|_{z=0,d} = 0, \; A \frac{\partial M_z}{\partial z}\Big|_{z=0,d} = 0$$

These equations correspond to a free or unpinned surface magnetization. We now have all of the boundary conditions which are required to solve the problem and the transmitted and reflected amplitudes can be calculated in a relatively straightforward manner by means of a digital computer.

Demonstration Curves

This section contains a series of curves which illustrate the dependence of the transmitted signal amplitude on the input parameters used in the calculation. The transmitted signal amplitude is defined to be the ratio of the transmitted to incident microwave magnetic fields.

Fig. 2.2 shows the transmitted amplitude as a function of the applied field for various values of the sample thickness. All of the other parameters have been set equal to the published values for bulk nickel at 300 K. The FMAR transmission peak is located at approximatly 1.7 KOe. The small peak at 5.5 KOe is the ultrasonic signal which is centered at FMR. The rise in the transmitted amplitude at higher fields is a result of the decrease in the permeability with increasing field (in the limit of very large fields $\mu = 1$ see equation 1.6).

Fig. 2.3 shows the transmitted amplitude as a function of sample thickness for various values of the ultrasonic decay time (tau). All of the other parameters have been set equal to the published values for bulk nickel at 300 K. The applied field is fixed at the peak of the FMR transmission (5.49 KOe). The peak in the transmitted amplitude at a thickness of 2.32 μm is a result of acoustic standing waves in the sample. It should be noted that a change in the value of c_{44} or the density (changes in the speed of sound) will cause a shift in the position of this peak.

Fig. 2.4 shows the transmitted amplitude as a function of applied field for various values of the magnetic damping parameter (gilbert). All of the other parameters have been set equal to the published values for bulk nickel at 300 K. Note that the FMR transmission signal decreases rapidly with increasing magnetic damping. The transmitted signal amplitude at FMR is approximately proportional to $1/G^2$.

Fig. 2.5 shows the transmitted amplitude as a function of applied field for various values of the magnetoelastic coupling parameter (B_2). All of the other parameters have been set equal to the published values for bulk nickel at 300 K. The maximum FMR signal amplitude is approximately proportional to the square of the magnetoelastic coupling

parameter (the coupling parameter enters once at each surface).

Fig. 2.6 shows the transmitted amplitude as a function of applied field for various values of sample restivity. All of the other parameters have been set equal to the published values for bulk nickel at 300 K.

Fig. 2.7 shows the transmitted amplitude as a function of applied field for various values of the magnetocrystaline anisotropy (K_1). All of the other parameters have been set equal to the published values for bulk nickel at 300 K. A change in the anisotropy constant simply shifts the whole curve rigidly to higher or lower fields.

Fig. 2.8 shows the transmitted amplitude as a function of applied field for various values of the sample magnetization (satmag). All of the other parameters have been set equal to the published values for bulk nickel at 300 K. Neglecting shifts due to damping, exchange and anisotropy the FMAR peak is located at a field $H_{FMAR} = \frac{\omega}{\gamma} - 4\pi M_s$ and FMR occurs at a field such that $(BH)^{.5} = \omega/\gamma$.

Fig. 2.9 shows the transmitted amplitude as a function of applied field for various values of the exchange constant, A. All of the other parameters have been set equal to the published values for bulk nickel at 300 K.

Fig. 2.10 shows the real and imaginary parts of the phonon wavevector as a function of applied field. The phonon lifetime (tau) is long enough so that essentially all of the ultrasonic absorption is a result of magnetoelastic coupling. The peak in absorption occurs at a field $2AK^2/M_s$ below FMR where K is the phonon wavevector. The separation between the peak in ultrasonic absorption and FMR is a result of spinwave dispersion [12,18]. The effect of changing the separation between FMR and the maximum in ultrasonic absorption can be seen in Fig. 2.9 where the exchange constant A (spinwave dispersion) has been varied.

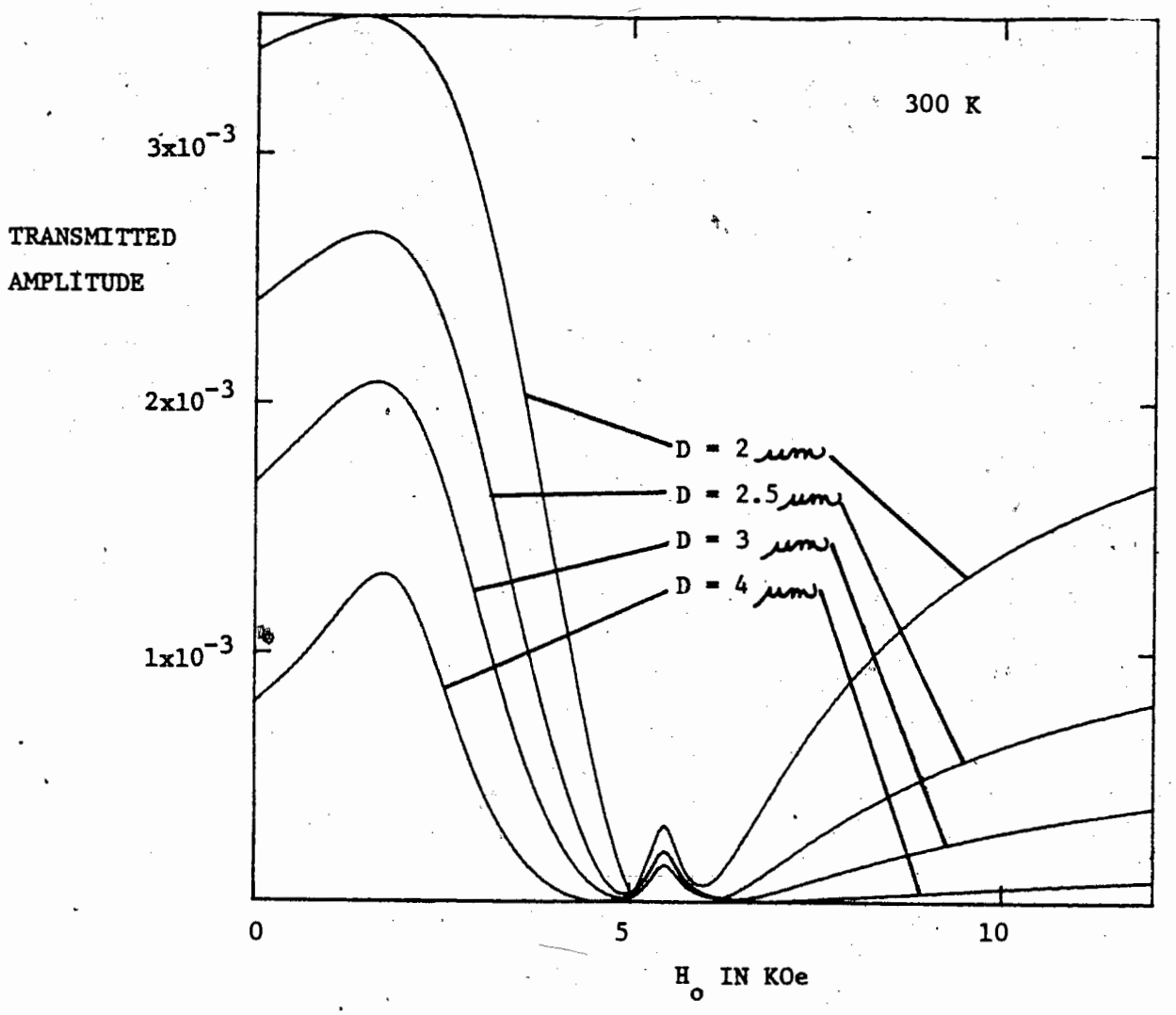

Fig. 2.2 Calculated transmission amplitude as a function of applied field for various values of the thickness d. The applied frequency was 23.943 GHz the other parameters used in the calculation were taken from the published values for nickel at 300 K. They were ω/γ =7.822 KOe, $4\pi M_s$=6.143 KOe, G=2.45 x 10^8 Hz, R=7.529 x 10^{-6} ohm-cm, A=1.0 x 10^{-6} ergs/cm, $2K_1/M_s$=-240 Oe, B_2=1.07 x 10^8 ergs/cm^3, density=8.906 g/cm^3, tau=.66 x 10^{-9} sec, and C_{44}=1.234 x 10^{12} ergs/cm^3.

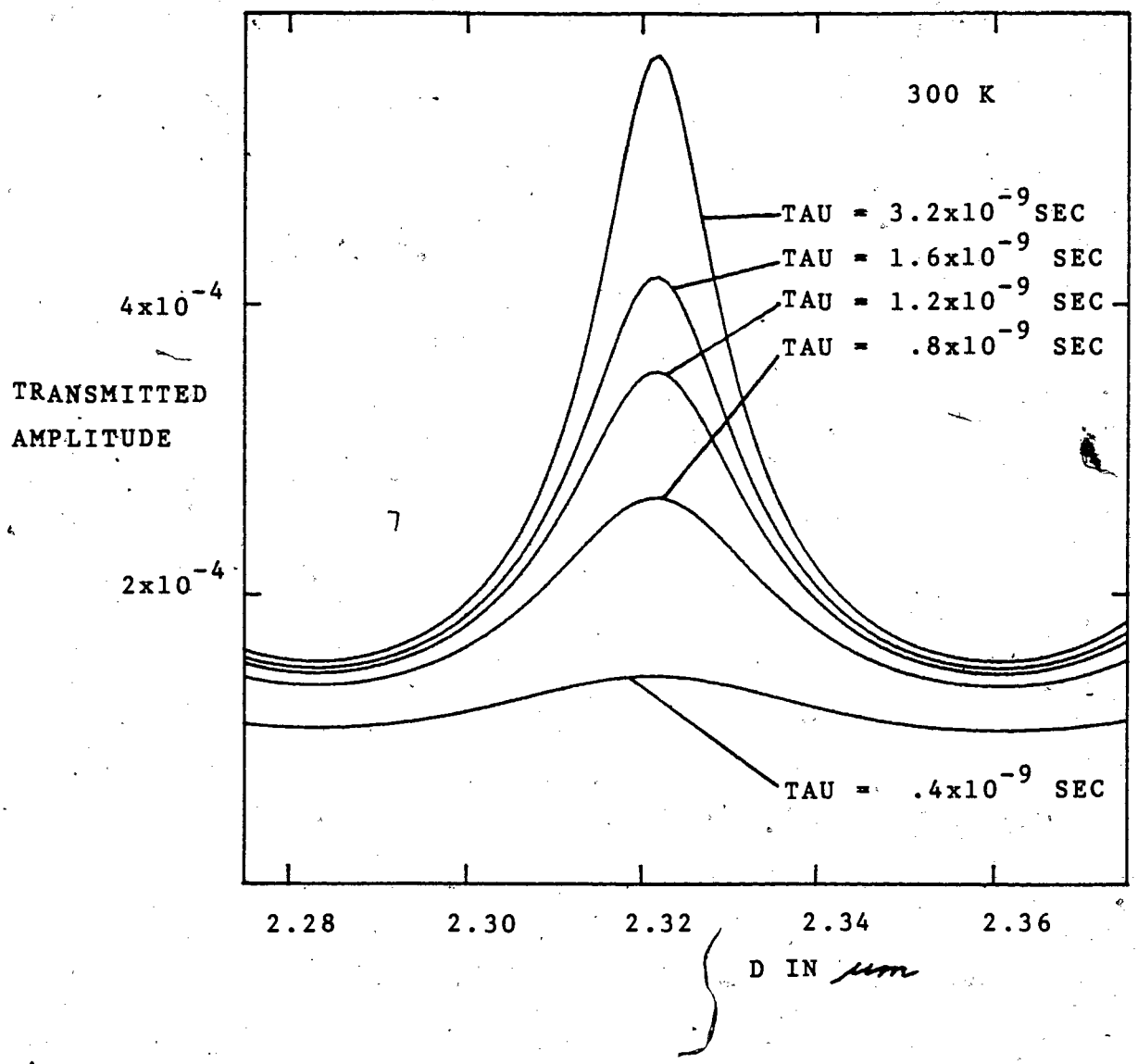

Fig. 2.3 Calculated transmission amplitude at 5.49 KOe as a function of sample thickness for various values of the ultrasonic decay time tau. The applied frequency was 23.943 GHz the other parameters used in the calculation were taken from the published values for nickel at 300 K. They were ω/γ =7.822 KOe, $4\pi M_s$=6.143 KOe, G=2.45 x 10^8 Hz, R=7.529 x 10^{-6} ohm-cm, A=1.0 x 10^{-6} ergs/cm, $2K_1/M_s$=-240 Oe, B_2=1.07 x 10^8 ergs/cm^3, density=8.906 g/cm^3, and C_{44}=1.234 x 10^{12} ergs/cm^3.

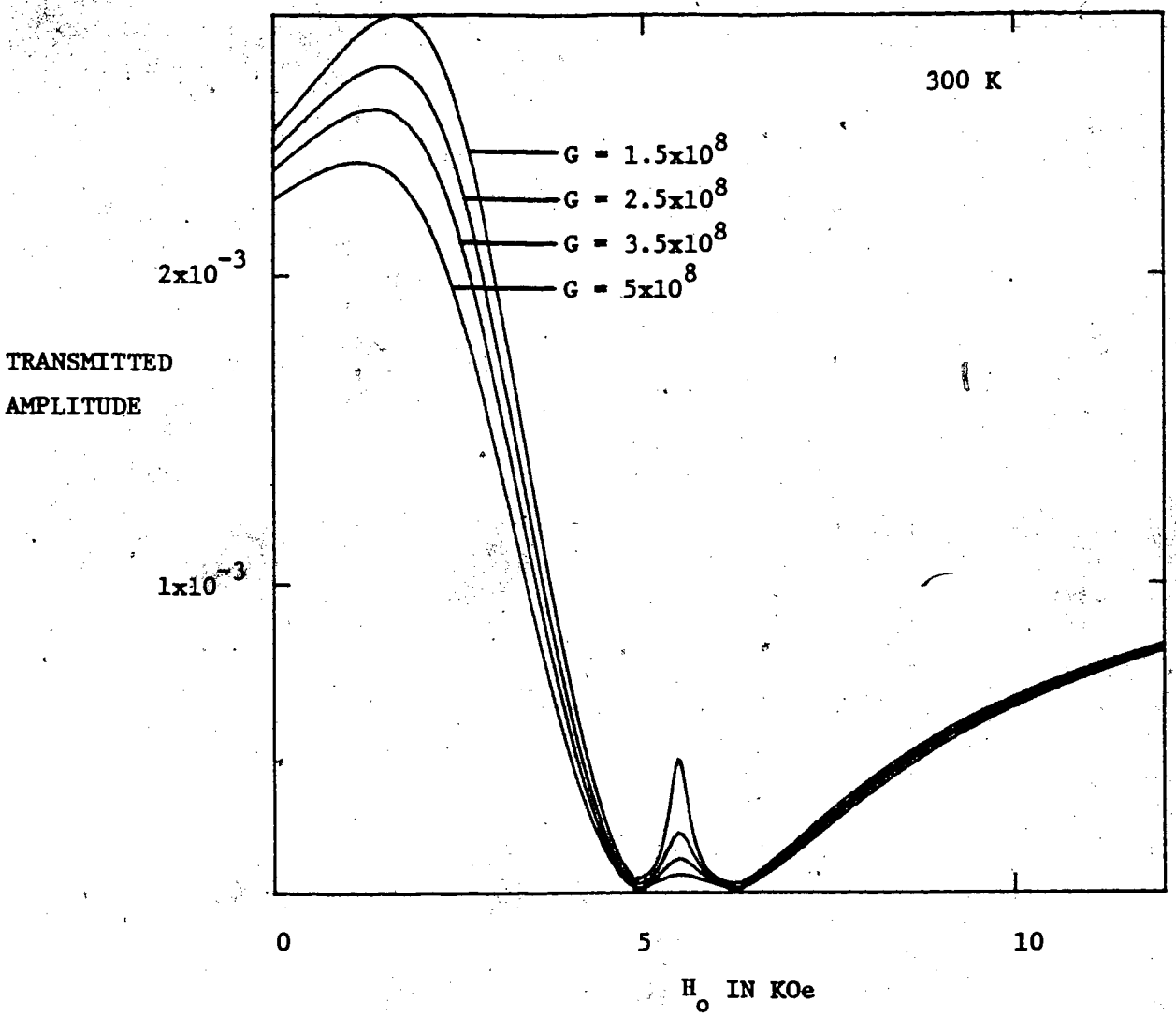

Fig. 2.4 Calculated transmission amplitude as a function of applied field for various values of the magnetic damping parameter G. The applied frequency was 23.943 GHz, the sample thickness was $d=2.5 \times 10^{-4}$ cm and the other parameters used in the calculation were taken from the published values for nickel at 300 K. They were $\omega/\gamma = 7.822$ KOe, $D=2.5 \times 10^{-4}$ cm, $4\pi M_s = 6.143$ KOe, $R=7.529 \times 10^{-6}$ ohm-cm, $A=1.0 \times 10^{-6}$ ergs/cm, $2K_1/M_s = -240$ Oe, $B_2 = 1.07 \times 10^8$ ergs/cm^3, density=8.906 g/cm^3, tau=.66 x 10^{-9} sec, and $C_{44} = 1.234 \times 10^{12}$ ergs/cm^3.

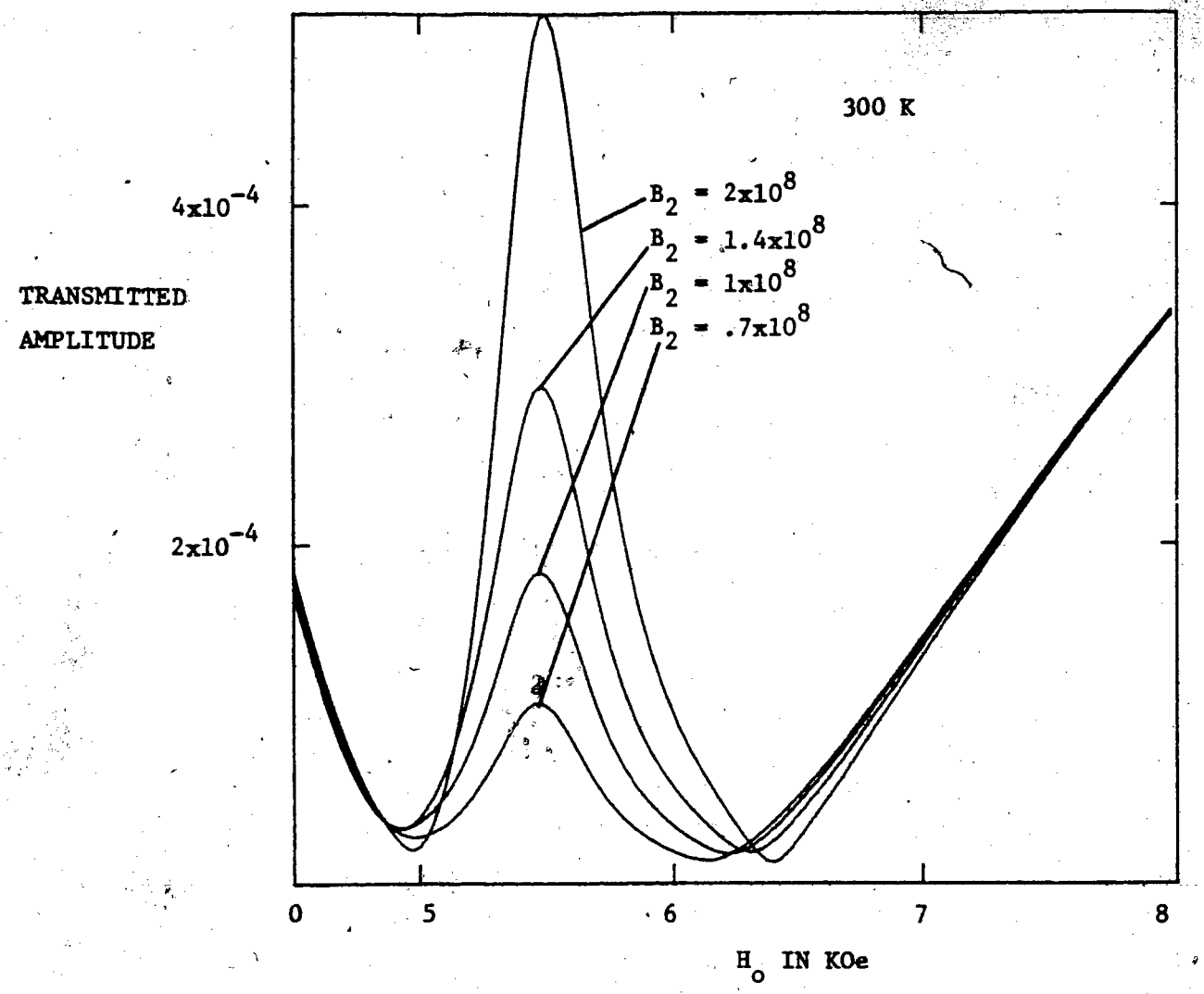

Fig. 2.5 Calculated transmission amplitude as a function of applied field for various values of the magnetoelastic coupling parameter B_2. The applied frequency was 23.943 GHz, the sample thickness was d=2.5 x 10^{-4}cm and the other parameters used in the calculation were taken from the published values for nickel at 300 K. They were ω/γ =7.822 KOe, D=2.5 x 10^{-4} cm, $4\pi M_s$=6.143 KOe, G=2.45 x 10^8 Hz, R=7.529 x 10^{-6} ohm-cm, A=1.0 x 10^{-6} ergs/cm, $2K_1/M_s$=-240 Oe, density=8.906 g/cm^3, tau=.66 x 10^{-9} sec, and C_{44}=1.234 x 10^{12} ergs/cm^3.

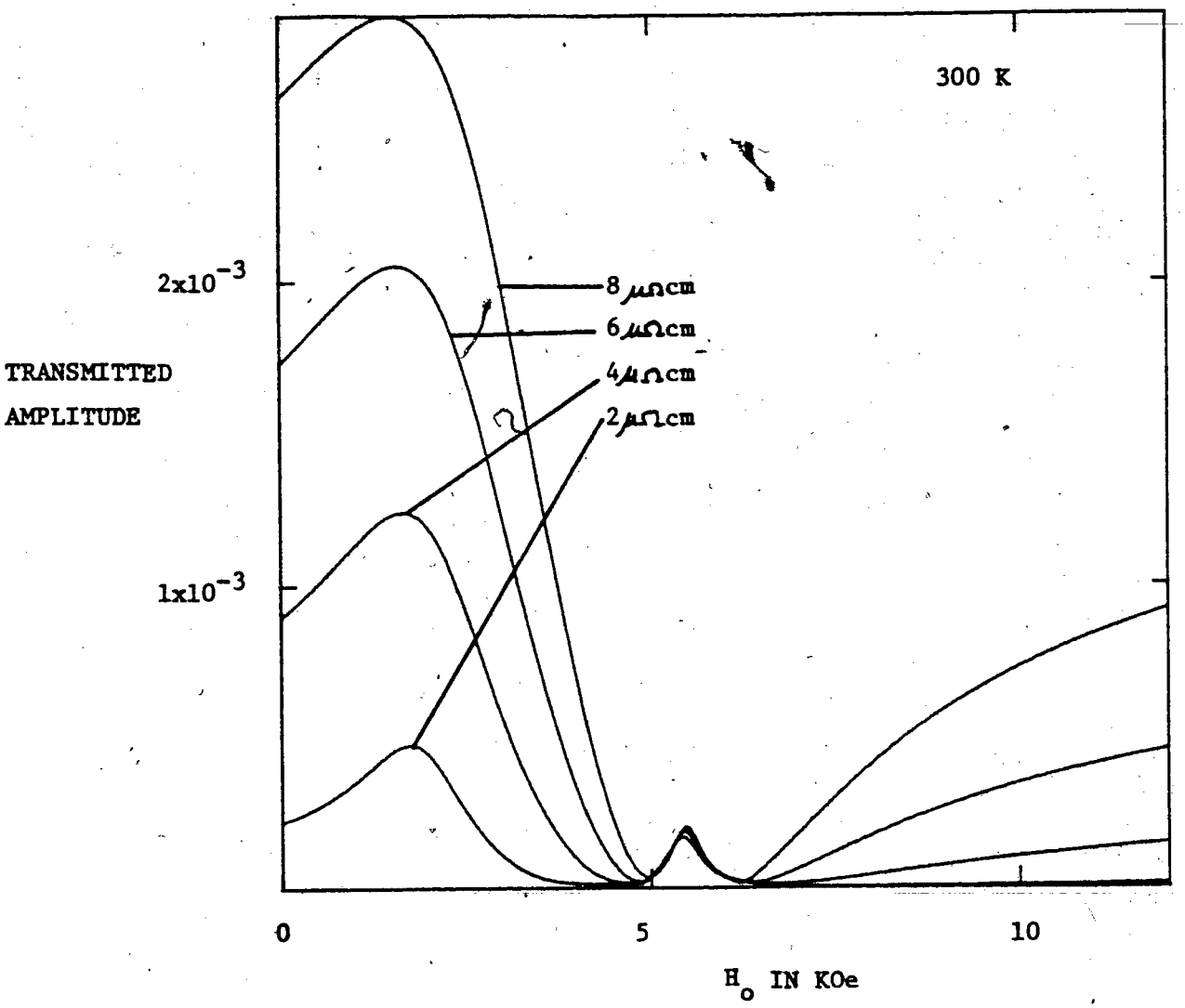

Fig. 2.6 Calculated transmission amplitude as a function of applied field for various values of the sample resistivity R. The applied frequency was 23.943 GHz, the sample thickness was $d=2.5 \times 10^{-4}$ cm and the other parameters used in the calculation were taken from the published values for nickel at 300 K. They were $\omega/\gamma = 7.822$ KOe, $D=2.5 \times 10^{-4}$ cm, $4\pi M_s = 6.143$ KOe, $G=2.45 \times 10^{8}$ Hz, $A=1.0 \times 10^{-6}$ ergs/cm, $2K_1/M_s = -240$ Oe, $B_2=1.07 \times 10^{8}$ ergs/cm^3, density=8.906 g/cm^3, tau=.66 x 10^{-9} sec, and $C_{44}=1.234 \times 10^{12}$ ergs/cm^3.

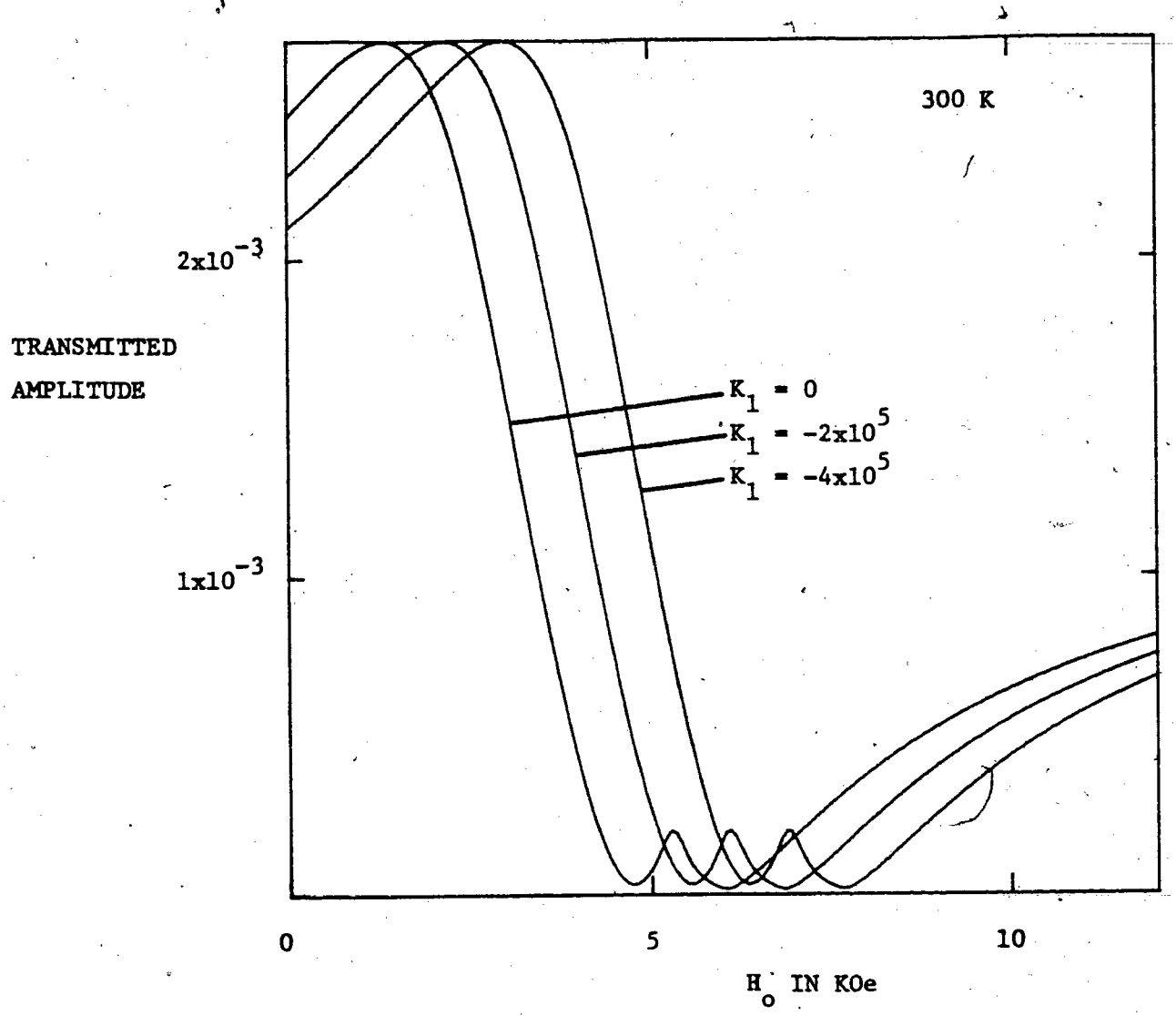

Fig. 2.7 Calculated transmission amplitude as a function of applied field for various values of the anisotropy field $H_{an}=2K_1/M_s$. The applied frequency was 23.943 GHz, the sample thickness was $d=2.5 \times 10^{-4}$cm and the other parameters used in the calculation were taken from the published values for nickel at 300 K. They were $\omega/\gamma = 7.822$ KOe, $D=2.5 \times 10^{-4}$ cm, $4\pi M_s = 6.143$ KOe, $G=2.45 \times 10^{8}$ Hz, $R=7.529 \times 10^{-6}$ ohm-cm, $A=1.0 \times 10^{-6}$ ergs/cm, $B_2=1.07 \times 10^{8}$ ergs/cm^3, density=8.906 g/cm^3, tau=$.66 \times 10^{-9}$ sec, and $C_{44}=1.234 \times 10^{12}$ ergs/cm^3.

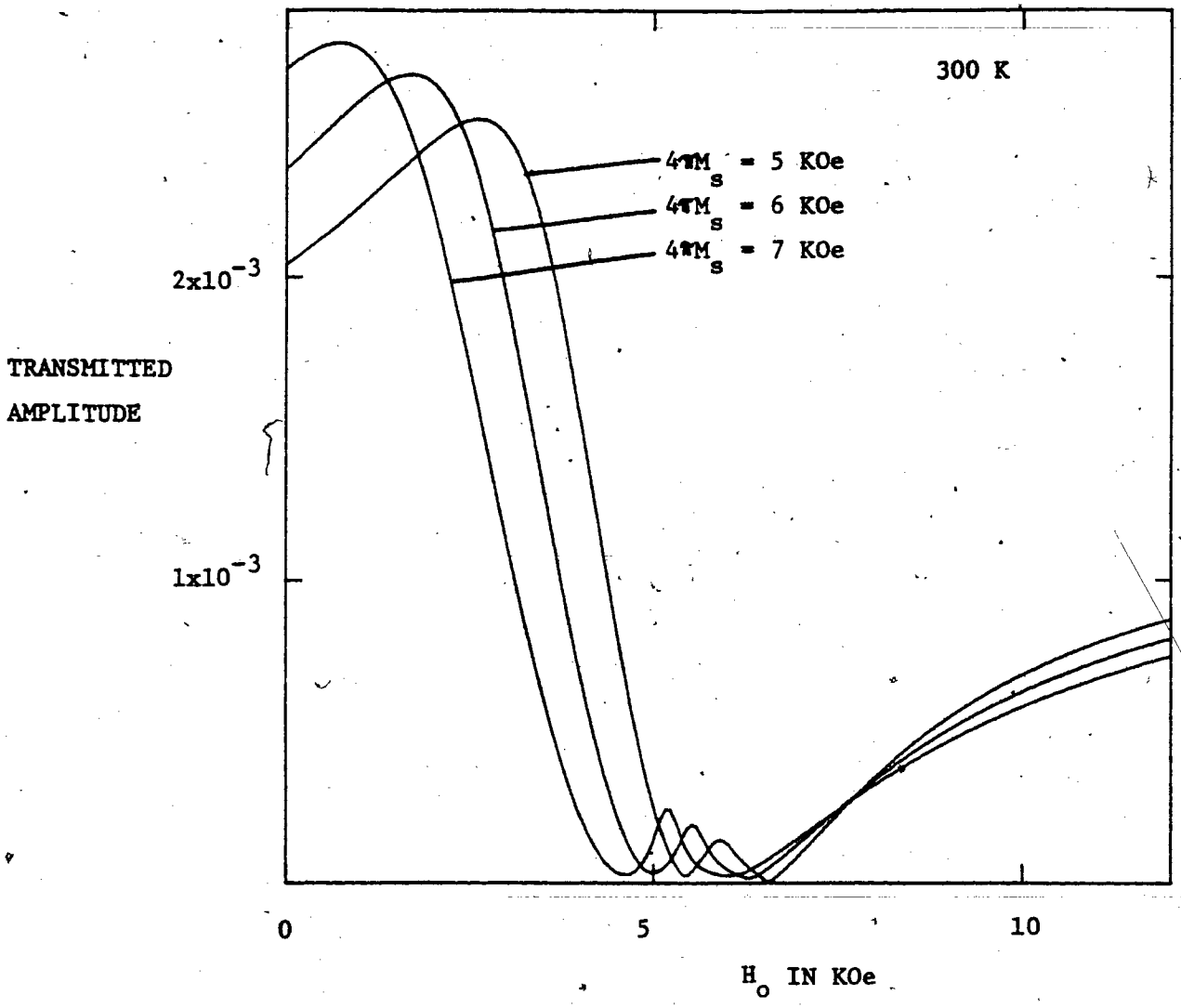

Fig. 2.8 Calculated transmission amplitude as a function of applied field for various values of the sample magnetization. The applied frequency was 23.943 GHz, the sample thickness was $d=2.5 \times 10^{-4}$cm and the other parameters used in the calculation were taken from the published values for nickel at 300 K. They were ω/δ =7.822 KOe, $D=2.5 \times 10^{-4}$ cm, $G=2.45 \times 10^{8}$ Hz, $R=7.529 \times 10^{-6}$ ohm-cm, $A=1.0 \times 10^{-6}$ ergs/cm, $2K_1/M_s=-240$ Oe, $B_2=1.07 \times 10^{8}$ ergs/cm^3, density=8.906 g/cm^3, tau=$.66 \times 10^{-9}$ sec, and $C_{44}=1.234 \times 10^{12}$ ergs/cm^3.

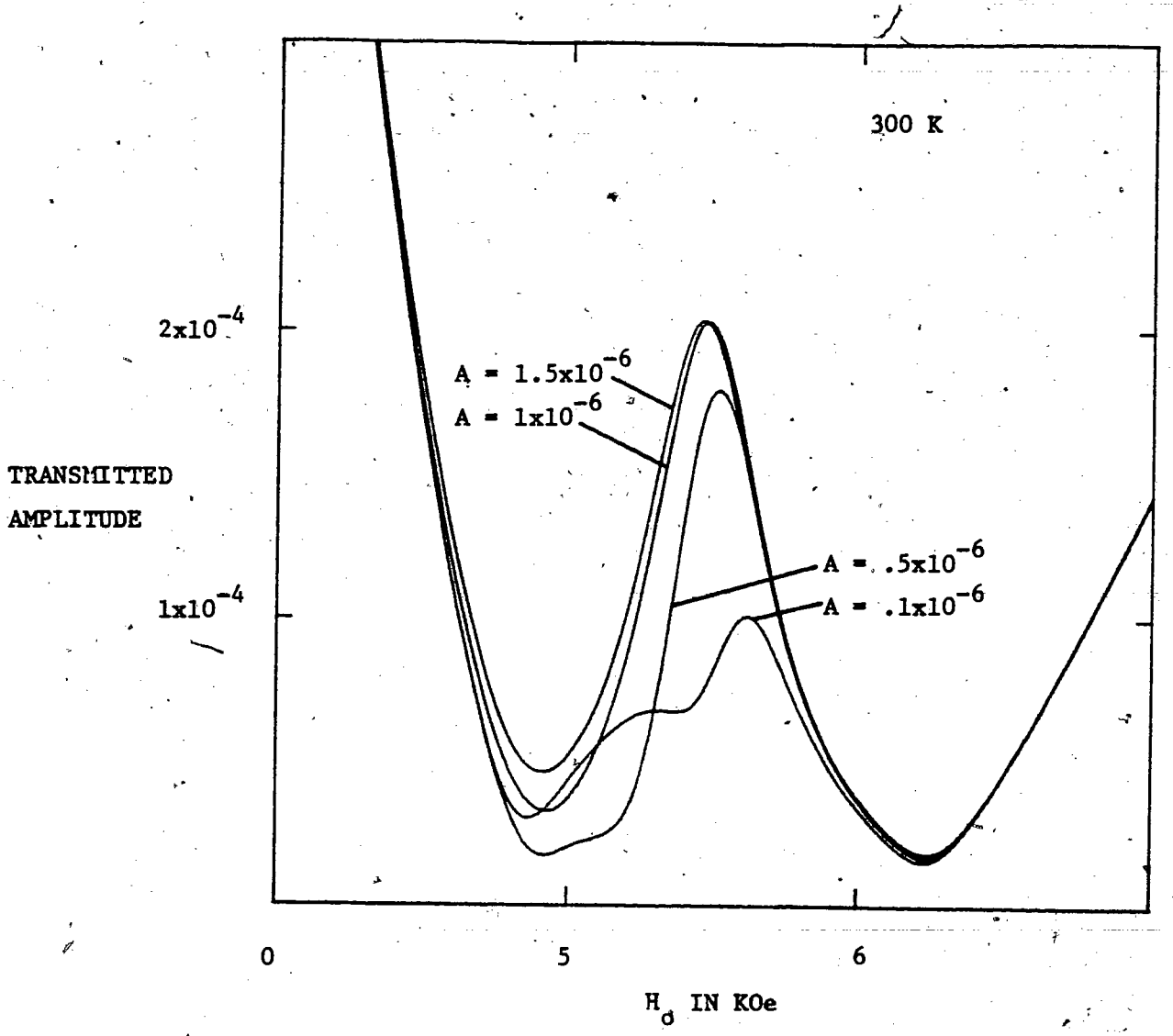

Fig. 2.9 Calculated transmission amplitude as a function of applied field for various values of the exchange stiffness parameter A. The applied frequency was 23.943 GHz, the sample thickness was $d=2.5 \times 10^{-4}$ cm and the other parameters used in the calculation were taken from the published values for nickel at 300 K. They were $\omega/\gamma = 7.822$ KOe, $D=2.5 \times 10^{-4}$ cm, $4\pi M_s = 6.143$ KOe, $G=2.45 \times 10^{8}$ Hz, $R=7.529 \times 10^{-6}$ ohm-cm, $2K_1/M_s = -240$ Oe, $B_2=1.07 \times 10^{8}$ ergs/cm^3, density=8.906 g/cm^3, tau=.66 x 10^{-9} sec, and $C_{44}=1.234 \times 10^{12}$ ergs/cm^3.

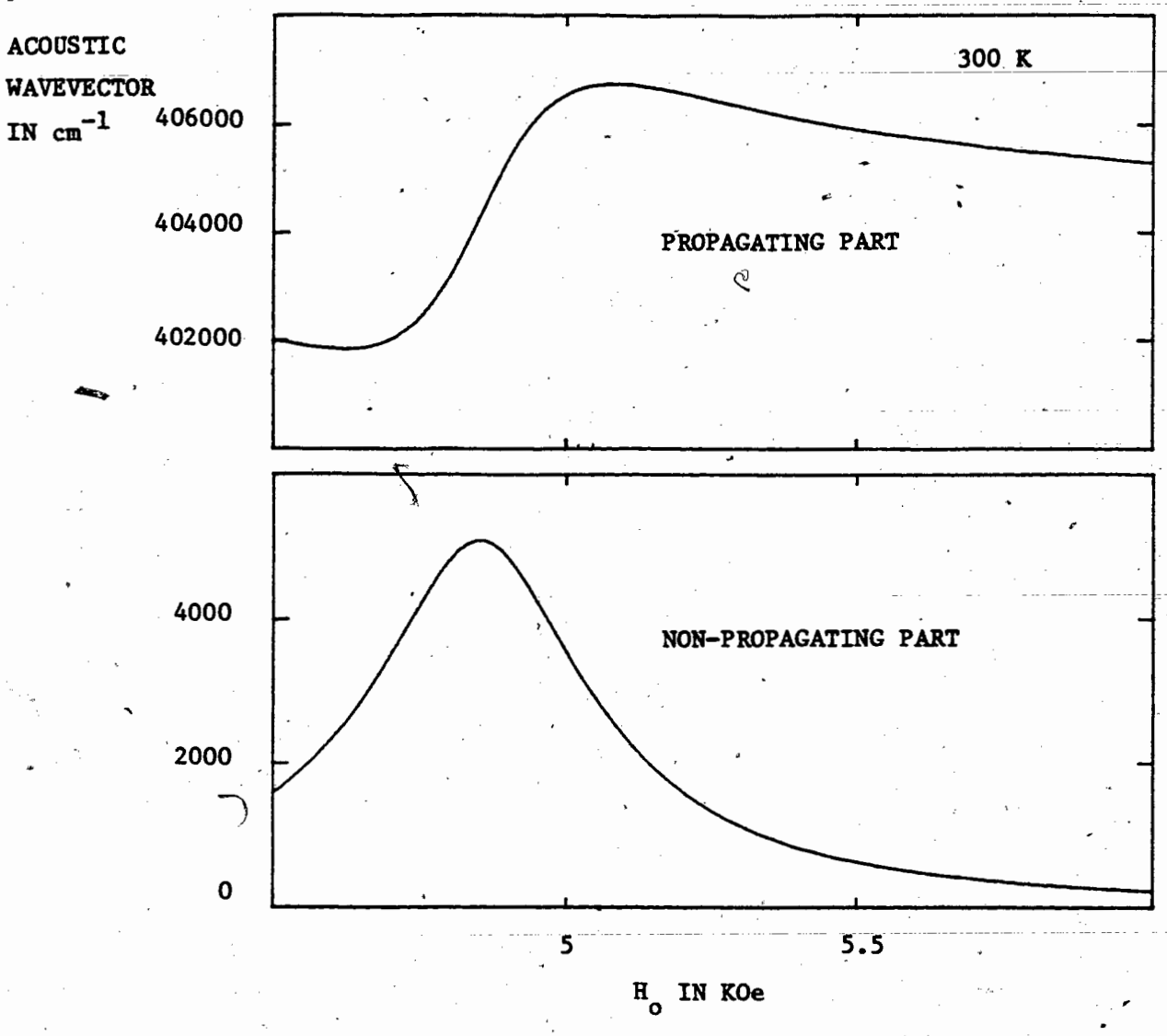

Fig. 2.10 The real and imaginary parts of the phonon wavevector as a function of the applied field. The applied frequency was 23.943 GHz, the sample thickness was $d=2.5 \times 10^{-4}$ cm and the other parameters used in the calculation were taken from the published values for nickel at 300 K. They were $\omega/\gamma = 7.822$ KOe, $D=2.5 \times 10^{-4}$ cm, $4\pi M_s = 6.143$ KOe, $G=2.45 \times 10^{8}$ Hz, $R=7.529 \times 10^{-6}$ ohm-cm, $A=1.0 \times 10^{-6}$ erg/cm, $2K_1/M_s = -240$ Oe, $B_2=1.07 \times 10^{8}$ ergs/cm^3, density=8.906 g/cm^3, tau=1×10^{-6} sec, and $C_{44}=1.234 \times 10^{12}$ ergs/cm^3.

III. EXPERIMENTAL DETAILS

Sample Preparation

In order to carry out low temperature transmission measurements it is necessary to have thin (2-3 μm) single crystal samples which are uniform in thickness over an area approximately 4 mm in diameter. A number of attempts were made to produce such samples by spark cutting slabs .5 mm thick from bulk single crystals and then mechanically polishing and finally electropolishing them down to the desired thickness. Unfortunately the resulting crystals tended to be thicker in the center then at the edges and were covered with a slight ripple ($\approx$ .2 μm amplitude) on both faces as a result of the electropolishing. Since crystals prepared in this way were not sufficiently uniform in thickness for our purposes we turned to crystals which were grown epitaxially by electrodeposition. These crystals were grown on a single crystal copper disk .5 mm thick and 2 cm in diameter using a technique similar to that described by Wright [11]. The copper substrates were spark cut from a single crystal boule obtained from Materials Research Corp. The resulting disks had the [110] axis normal to their face. One of the faces was prepared for electrodeposition by mechanically polishing, by proceeding from 400 grit silicon carbide paper to 1 μm diamond grit embedded in a paper lap. Although the resulting surface was mirror-like, the mechanical polishing leaves a thin layer of highly deformed copper on the surface. This layer was removed by electropolishing the copper in a 36% by volume H_3PO_4 [19] solution at a current density of .4 amp per cm^2. During the polishing the surface of the

crystal was continuously rubbed with a cotton swab to prevent bubbles from adhering. It was found that this solution tended to produce a slightly rippled surface if it was allowed to polish for a long time. In order to minimize this effect the electropolishing should not be continued for more than one minute. The substrate was removed from the polishing solution without disconnecting the current, and was then thoroughly rinsed in distilled water while making sure that the surface always remained wet. As the crystal growth was not carried out in an inert atmosphere the time spent in transfering the polished copper disc from the polishing solution to the plating cell should be kept to a minimum (< 15 sec.). However, even during this short period an oxide layer will likely have formed on the copper substrate. Such an oxide layer could prevent epitaxial growth. Fortunately a thin oxide layer may be removed during the initial stages of deposition by the reaction [20]

$$Cu_2O + 2H^+ + 2e^- \rightleftharpoons 2Cu + H_2O \ .$$

The clean copper substrate was placed in a plating cell containing a cobalt sulphate solution at 18C which consisted of 300 g/l $CoSO_4.7H_2O$, 6 g/l H_3BO_4 and 3 g/l NaCl which had been adjusted to a ph of 2.3 by the addition of H_2SO_4 [21]. This solution had been filtered and boiled in a vacuum to remove any dissolved gasses before being placed in the cell. (An aspirator was used to create the vacuum.) The substrate was then plated for 60 seconds at a current density of 12 ma/cm^2. This produced a shiny layer of face centered cobalt approximately .1 μm thick.

Upon removal from the cobalt solution the crystal was rinsed in distilled water and placed in a second plating cell which contained a nickel sulphate solution consisting of .43 m/l $NiSO_4.6H_2O$ and .4 m/l H_3BO_4 which had been adjusted to a ph of 3.7 by the addition of H_2SO_4 and which

was heated to a temperature of 27 C [22]. This solution had also been filtered and boiled in vacuum before being placed in the plating cell. The crystal was deposited at a current density of 20 ma/cm^2, a plating time of 9 minutes yielded $\approx$ 2.3 μm of nickel. Occasional agitation during plating was required to prevent the formation of pits due to bubbles on the surface.

The plating cell consisted of a rectangular plexiglas box 10 cm long by 5 cm wide by 7 cm deep which was divided in the middle by a sintered glass filter. The copper substrate was placed at one end and an anode made of the metal to be plated was at the other. The sintered glass filter was necessary to prevent particles which were etched free from the anode from reaching the cathode and disrupting the crystal growth [23].

There were two reasons for applying a thin cobalt layer to the copper substrate. The first was that face centered cobalt has a lattice constant between that of copper and nickel, this should help to reduce the amount of strain in the nickel crystal.

Table 1

	Lattice constant (20 C)[24]	Ratio to nickel
Cu	3.615 Å	1.0259
Co (fcc)	3.544 Å	1.0059
Ni	3.524 Å	1.0

Secondly it was hoped that the nickel foils could be removed from the copper substrate by dissolving the cobalt layer [11]. Unfortunately foils obtained in this way contained numerous holes and hence were not suitable for transmission measurements. It should be noted that we have also grown nickel directly on copper but we have not yet been able to determine which

method results in better crystals.

As was mentioned earlier, the nickel crystal could not be removed by dissolving the cobalt layer so the copper substrate and the thin cobalt layer were removed from the nickel crystal. This was done by electropolishing away the bulk of the copper. During this process the nickel was protected by a layer of beeswax. The remainder of the copper substrate and the cobalt film were dissolved away by means of a chromic acid solution consisting of 500 g/l CrO_3 and 50 g/l H_2SO_4 [25]. This solution seems to have no effect on the nickel crystal. Specimens 4 mm on a side were cut from the resulting nickel single crystal foil and were annealed in vacuum at 1000 C for 6 hours. After which they were ready to be mounted.

Microwave System

All of the microwave measurements were carried out using a 24 GHz homodyne system which has previously been described in detail [16]. This system has a sensitivity of approximately 10^{-17} watts in a 1 Hz bandwidth. In order to mount the specimen it was soldered using pure indium over a 1.8 mm diameter orifice in a .15 mm thick beryllium copper diaphragm. This diaphragm was then mounted to form a common wall between tuned transmitter and receiver cavities. Spurious leakage between the cavities was prevented by means of a gasket formed from .4 mm diameter indium wire. The cavities were mounted in an electromagnet in such a way that the applied field could be rotated in the plane of the sample. As most of the measurements were to be made below room temperature a double wall liquid nitrogen shielded dewar was placed around the cavities. The cavities were cooled by blowing cold nitrogen gas over them. The temperature was

regulated by means of a small heater strapped to the lower cavity. Liquid helium was used to reach temperatures below 77K.

Although the crystal had been oriented by means of a Laue x-ray photograph it was still necessary to determine the exact orientation of the crystal axis relative to the applied magnetic field. The orientation of the crystal could easily be determined by measuring the position of FMR as a function of the magnet angle after the sample had been cooled so as to increase the value of the magnetocrystalline anisotropy. A maximum in the value of the applied field at which FMR occurs in Nickel is observed when the applied field is parallel to the [100] axis. Using this method it was possible to align the magnet to within 2° of the [100] axis by cooling the crystal to 150 K (the [110] axis was normal to the plane of the sample).

Before presenting the results of the microwave transmission measurements I would like to outline the procedure used to obtain a complete set of transmission measurements. First the magnet was aligned so that the applied field was along one of the crystal axes (usually [100]) and the klystron frequency was locked to that of an external reference cavity. Once the temperature of the sample had reached the desired value the transmitter and receiver were tuned to the klystron frequency by means of quartz tuning rods inserted into each cavity. As the samples measured were relatively thin it was necessary to insert an attenuator in the wave guide leading to the transmitter cavity in order to prevent the signal from overloading the mixer. Next the microwave phase shifter was adjusted for the first phase and the signal amplitude was then recorded as a function of applied magnetic field. The data was stored both on an analog x-y chart recorder and digitally using a PDP-8 based microcomputer. After the signal had been recorded over the desired field region two additional measurements were made. First the magnet was rotated so that the applied

D.C. magnetic field was parallel to the microwave magnetic field and the D.C. field was adjusted to approximately 10 KOe. In this configuration the R.F. permeability is equal to unity and the amplitude of the transmitted signal depends only on the thickness and conductivity of the sample. Throughout the rest of this thesis this signal will be referred to as the parallel parallel signal. A second measurement was made with the attenuator in the waveguide leading to the transmitter cavity closed. This measurement was used to digitally subtract any signal resulting from leakage between waveguides. This completed the measurement of the first phase. The phase shifter was then moved by 90° and all the measurements were repeated. As a final step the data was transferred from the microcomputer to an IBM 4341 where the total transmitted signal amplitude was calculated by digitally combining the signals corresponding to the two phases.

IV. EXPERIMENTAL RESULTS

The bulk of the experimental data is in the form of a series of measurements of the transmitted amplitude as a function of the applied magnetic field. In order to extract information about the properties of Ni from the observed transmission curves the parameters used to calculate the transmitted signal were varied until a good fit was secured to the observed signal. Each experimentally observed transmission curve is presented along with a theoretical fit. In order to make a theoretical fit to the observed transmission signal we need to know both the resistivity and thickness of the sample. The resistivity was determined by measuring the resistance of a strip approximately 1 mm wide and 1 cm long cut from a section of the crystal which was adjacent to the specimen used for the transmission measurements. The resistance of this strip was measured at room temperature, in liquid Nitrogen (77 K) and in liquid Helium(4.2 K) using a standard 4 probe technique. The resistance of the sample was assumed to be given by the sum of a constant residual resistance and the resistance that would be observed in a pure Nickel sample [26,27,28]. The magnitude of the residual resistance was in this way found to have the values shown in Table 2.

Table 2

	R/R_{299}	Residual Resistance
299 K	1	na
LN_2(77 K)	8.93	.295 $\mu\Omega$ cm
LHe(4.2K)	24.4	.307 $\mu\Omega$ cm

As can be seen in Table 2 the values of R_R obtained from R_{77}/R_{299} and $R_{4.2}/R_{299}$ agree very well. A value for the residual resistance of R_R=.307 $\mu\Omega$ cm was used throughout the rest of this work since the value for the residual resistance obtained from the 77 K measurement could be strongly affected by a small change in the temperature of the sample.(A .7 degree difference in temperature would account for the observed discrepancy) It appears that a large portion of the residual resistance is associated with the annealing process. We have made measurements of the residual resistance ratio of nickel crystals which had been grown directly on the copper substrate. Before annealing these samples had a residual resistance ratio of over 200 this ratio dropped to about 20 after they had been annealed. At this time the cause of the increased resistance is not known.

Sample Thickness

In order to determine its thickness, the sample was weighed using a Cahn Electrobalance and its area was estimated by using the stage on a metalographic microscope. These measurements along with a room temperature

density of 8.906 g/cm^3 [26,29] gave an average thickness of 2.5 μm. However the thickness of the crystal was found to increase towards the rim and so the value of 2.5 μm is likely to be an overestimate of the thickness at the centre of the sample. Fortunately one can quite accurately determine the thickness of the sample by making fits to the observed transmission amplitude. This is illustrated in Figures 4.1-3 where the thickness used in the calculation was varied from 2.275 to 2.375 μm. All of the other parameters used in the calculation are those for bulk Nickel at this temperature (300 K). As can be seen this is quite a sensitive means of determining the thickness. Another method for determining the sample thickness is to use the temperature dependence of the parallel parallel signal. The size of this signal depends only on the resistivity and thickness of the sample. Since we have already measured the resistivity we can determine the thickness. Fig. 4.4 shows the experimental data along with a fit obtained using a thickness of 2.31 μm. Although the data is somewhat noisy due to the difficulty in determining the sensitivity of the system as a function of temperature the results are consistent with those obtained by fitting the field dependence of the room temperature transmission signal. There is one last method which can be used to determine the sample thickness. This is to look for the presence of acoustic standing waves in the sample. Figures 4.5-7 show the transmitted amplitude at FMR as a function of sample thickness, the levels of the experimentally observed amplitudes are also shown. From Fig. 4.5 we see that the room temperature sample thickness must lie in the range 2.305 to 2.335 μm and from Fig. 4.7 we see that the sample thickness must lie between 2.278 and 2.308 μm or 2.283 to 2.313 μm at room temperature (allowing for .005 μm of thermal expansion). A room temperature thickness of 2.31 μm (2.305 μm at 100 k) would account for the observed

signal amplitudes. As a result of all these measurements a value of 2.310 μm was taken for the sample thickness.

Now having determined both the thickness and the resistivity of the sample we can investigate the temperature dependence of the magnetic damping and of the ultrasonic signal. Figures 4.8-16 show both the experimentally observed signal and a theoretical fit at each temperature. Only three free parameters were used to make a fit to the observed signals. These were:

1. The value of damping in the region of FMR (G_{FMR}).
2. The value of damping used elsewhere (G).
3. The value of the lifetime of the phonons (tau).

All other parameters used were obtained from the published values for Nickel (restivity[26,27,28],density [26,29],elastic constants [30],magnetocrystalline anisotropy [31], magnetization [32,33], magnetoelastic coupling constant [34]). It was found that a magnetic damping at FMR which was $.7 \times 10^8$hz larger than the values reported by Bhagat and Lubitz [3] gave a good fit to the observed linewidth at all temperatures. This value was used throughout the remainder of the thesis. In order to secure a fit to the data the following procedure was used.

At temperatures above approximately 150 K the experimental and calculated curves were scaled to have the same amplitude at FMAR. The value of G used was then adjusted until both curves agreed in the neighbourhood of FMAR and in the field region well above FMR (in this field region the signal is relatively insensitive to the value of G). After this had been done the relative scaling of the experimental and calculated curves was fixed and Tau was adjusted to match the amplitude of the FMR phonon peak.

For temperatures below 150 K the signal in the field region above FMR was not large enough to be used as a reference to fix the value of G_{FMAR}. It was therefore necessary to fix the relative size of the experimental and calculated signals by making use of the measured sensitivity of the system. Having fixed the relative scaling, the value of G was adjusted to give the correct amplitude at FMAR. Tau was then adjusted to match the amplitude of the FMR phonon peak.

The temperature dependence of the system sensitivity was determined by replacing the sample with a Be-Cu diaphragm which contained a small pinhole. As the coupling between cavities produced by such a pinhole should be temperature independent, any changes in the transmitted signal could be attributed to the temperature dependence of the system sensitivity. It was found that there was only a 10% variation in the sensitivity for temperatures below 200 K.

Fig. 4.17 shows the temperature dependence of the magnetic damping (G) measured in the region of FMAR. Also shown is a solid curve which represents the data obtained by Heinrich, Meredith, and Cochran. Unfortunately it was not possible to extend the present measurements to lower temperatures in spite of the fact that the crystal used in this work was approx 1/2 as thick as the one used by Heinrich, Meredith and Cochran. This was because the FMR transmission peak became so large relative to the FMAR signal that it dominated and obscured the FMAR signal at temperatures below 100 k. As a consequence, it was impossible to determine the damping parameter G which characterized the FMAR signal for temperatures less than 100 K. Fig. 4.18 shows the temperature dependence of the transmitted amplitude at FMR. The observed ultrasonic signal amplitude could be accounted for by using an ultrasonic decay time (tau) which had a value between .9 nsec and 1.4 nsec as is shown in Fig. 4.8-4.16 There are a

number of factors which contribute to the uncertainty in tau. First the transmitted amplitude depends strongly on the value of the magnetic damping (approximately like $1/G^2$) and so a relatively small error in the magnetic damping produces a large change in tau. Since acoustic interference effects were present it was necessary to accurately know the sample thickness, density and the shear modulus in order to determine tau. There was an uncertainty of .5% in the shear modulus [30] (this is equivalent to an uncertainty of .25% in the sample thickness) and as can be seen from Fig. 4.5-7, this can introduce a considerable uncertainty in the value of tau. And so to within experimental error (-25%, +100%) the ultrasonic decay time was found to have a temperature independent value of 1.2 nsec.

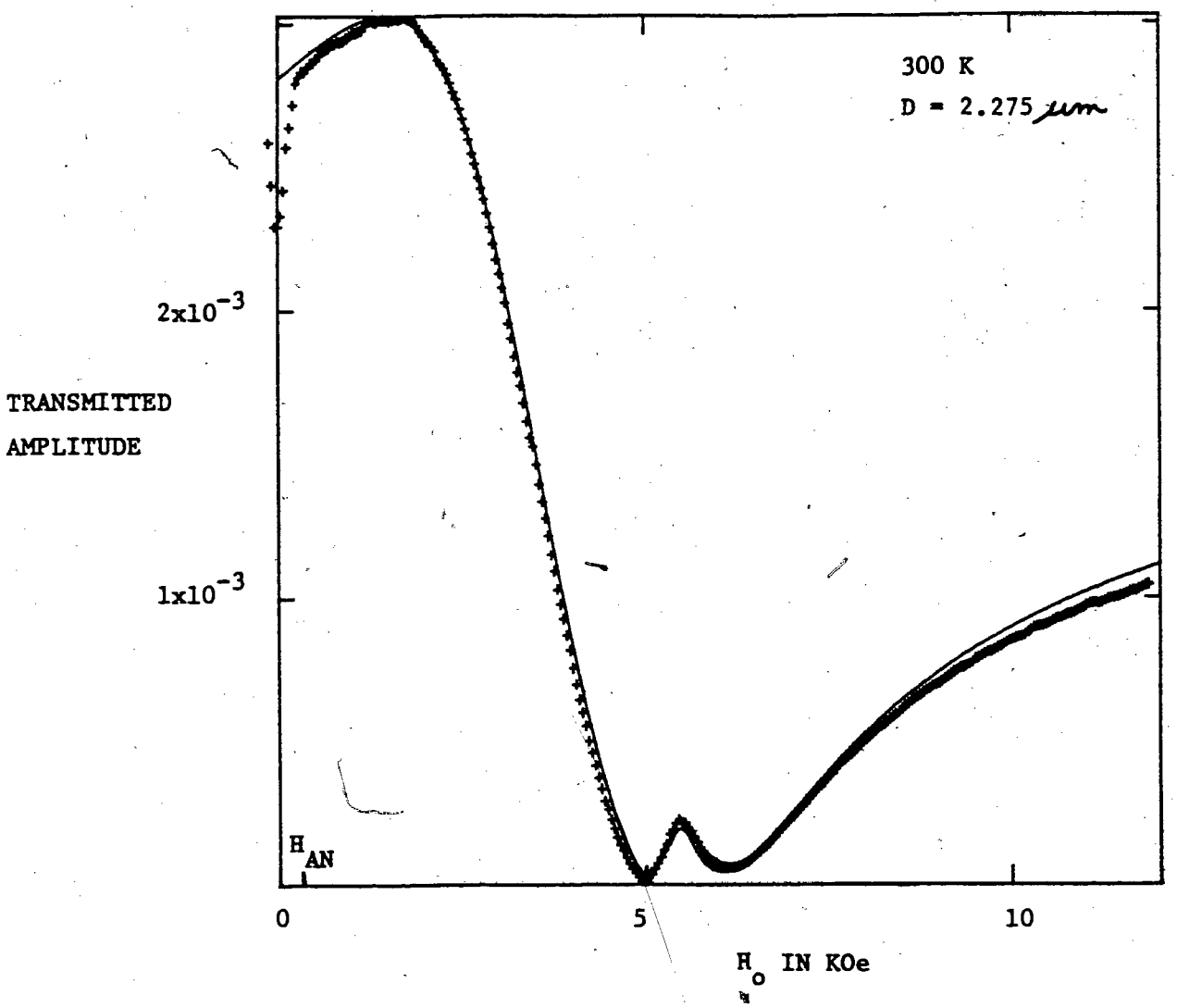

Fig. 4.1 The transmission amplitude as a function of the applied field. The crosses (+) represent experimental data and the solid line was calculated using R=7.529 μohm-cm, F=23.943 GHz, ω/γ =7.822 KOe, $4\pi M_s$=6.143 KOe, $2K_1/M_s$=-240 Oe, D=2.275 μm, A=1 x 10^{-6} ergs/cm, B_2=1.07 x 10^8 ergs/cm^3, density=8.9055 g/cm^3, G=2.45 x 10^8 Hz, C_{44}=1.234 x 10^{12}, and tau=.66 x 10^{-9}.

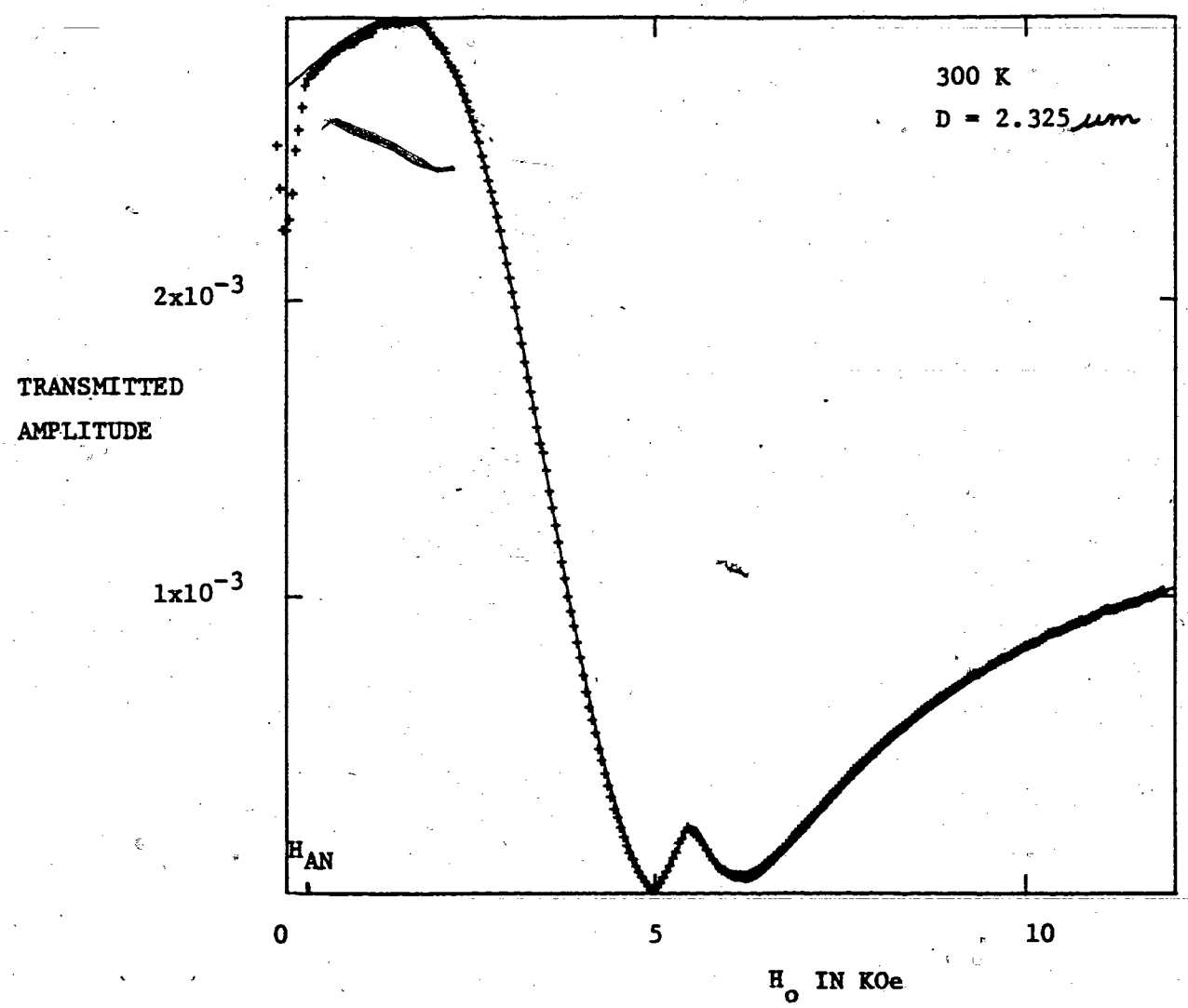

Fig. 4.2 The transmission amplitude as a function of the applied field. The crosses (+) represent experimental data and the solid line was calculated using R=7.529 μ ohm-cm, F=23.943 GHz, ω/γ =7.822 KOe, $4\pi M_s$=6.143 KOe, $2K_1/M_s$=-240 Oe, D=2.325 μm, A=1 x 10^{-6} ergs/cm, B_2=1.07 x 10^8 ergs/cm^3, density=8.9055 g/cm^3, G=2.45 x 10^8 Hz, C_{44}=1.234 x 10^{12}, and tau=.66 x 10^{-9}.

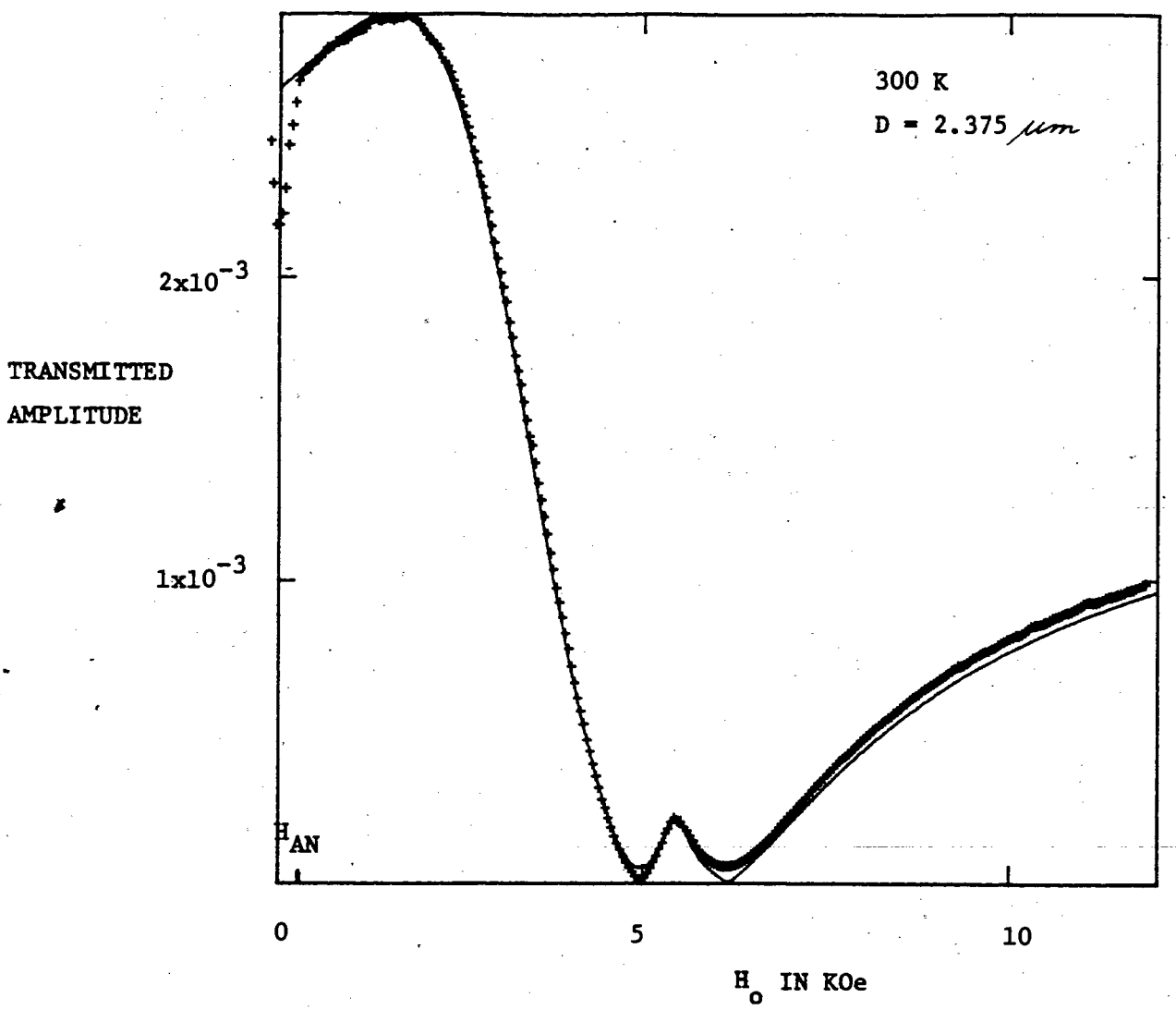

Fig. 4.3 The transmission amplitude as a function of the applied field. The crosses (+) represent experimental data and the solid line was calculated using R=7.529 μohm-cm, F=23.943 GHz, ω/γ =7.822 KOe, $4\pi M_s$=6.143 KOe, $2K_1/M_s$=-240 Oe, D=2.375 μm, A=1 x 10^{-6} ergs/cm, B_2=1.07 x 10^8 ergs/cm^3, density=8.9055 g/cm^3, G=2.45 x 10^8 Hz, C_{44}=1.234 x 10^{12}, and tau=.66 x 10^{-9}.

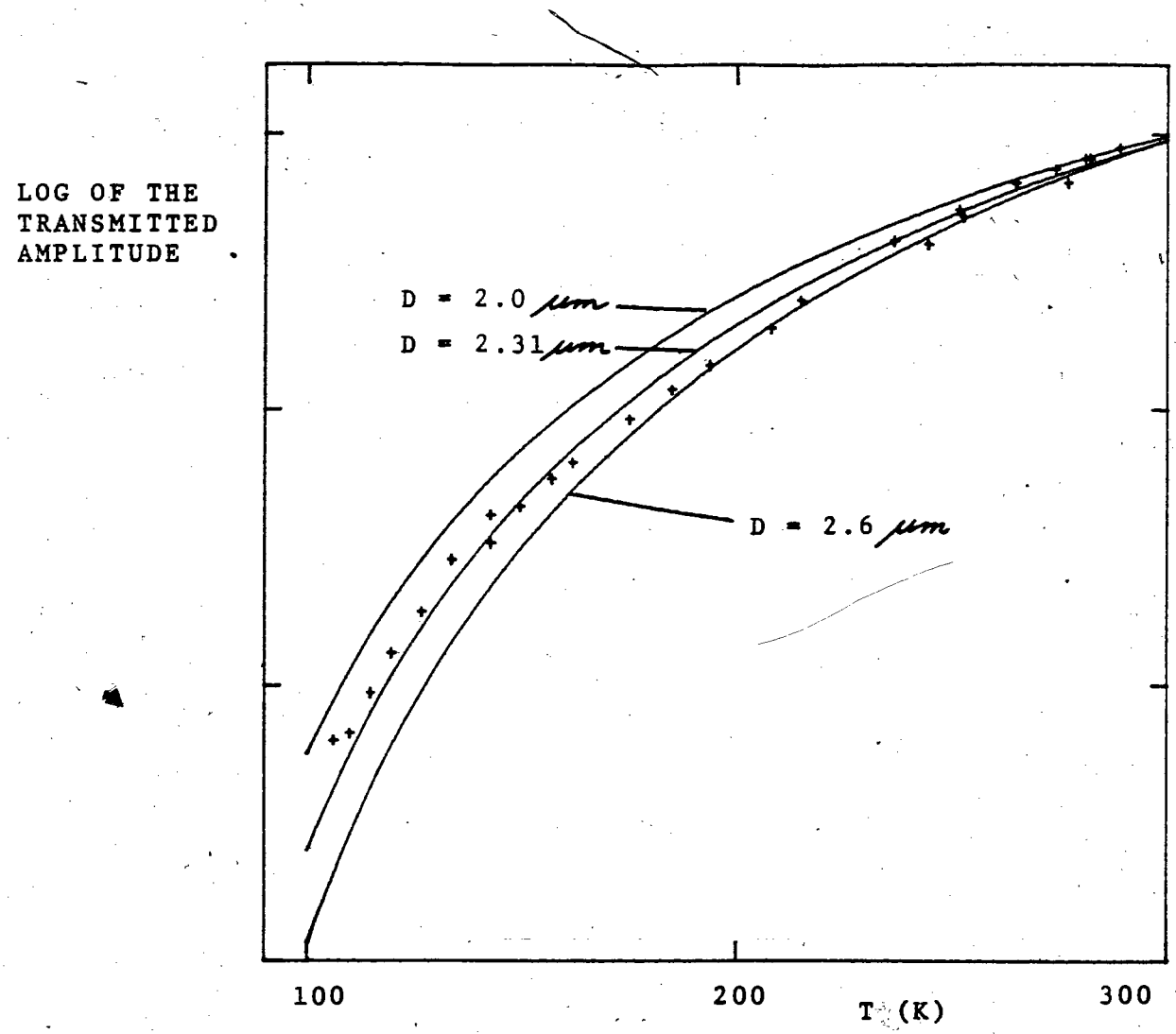

Fig. 4.4 The log of the transmitted amplitude as a function of temperature when the DC and microwave magnetic fields are applied in the same direction. (In this orientation the transmitted signal amplitude depends only on the thicknes and resitivity of the sample.) The crosses (+) represent experimental data and the solid lines were calculated using sample thicknesses of 2.0 μm ,2.31 μm and 2.6 μm.

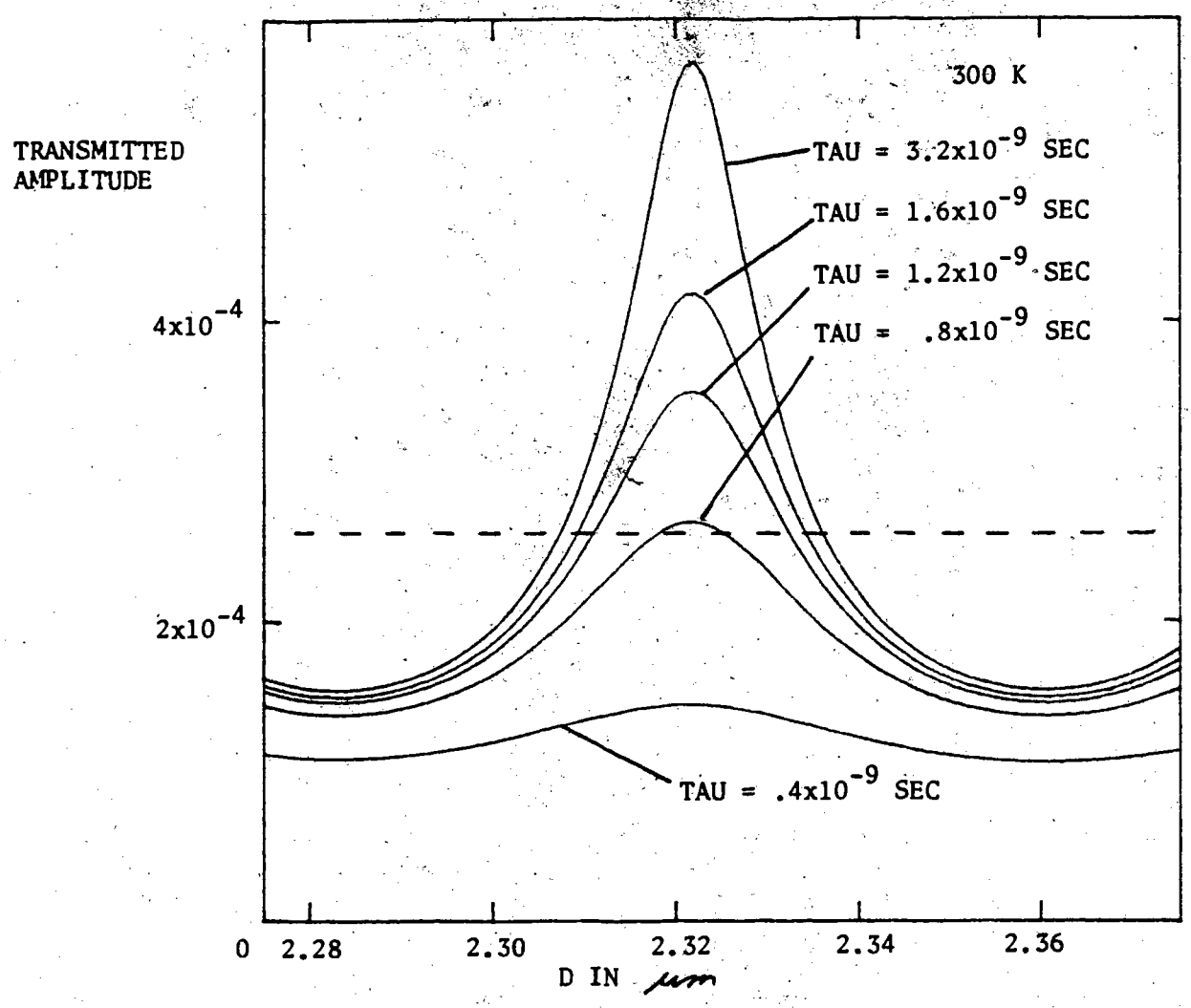

Fig. 4.5 The transmitted amplitude at FMR as a function of sample thickness for various values of tau. The dashed line shows the experimentally observed signal strength and the solid lines were calculated using R=7.529 μ ohm-cm, F=23.943 GHz, ω/γ =7.822 KOe, $4\pi M_s$=6.143 KOe, $2K_1/M_s$=-240 Oe, H_o=5.49 KOe, A=1 x 10^{-6} ergs/cm, B_2=1.07 x 10^8 ergs/cm^3, density=8.9055 g/cm^3, G=2.45 x 10^8 Hz and C_{44}=1.234 x 10^{12}.

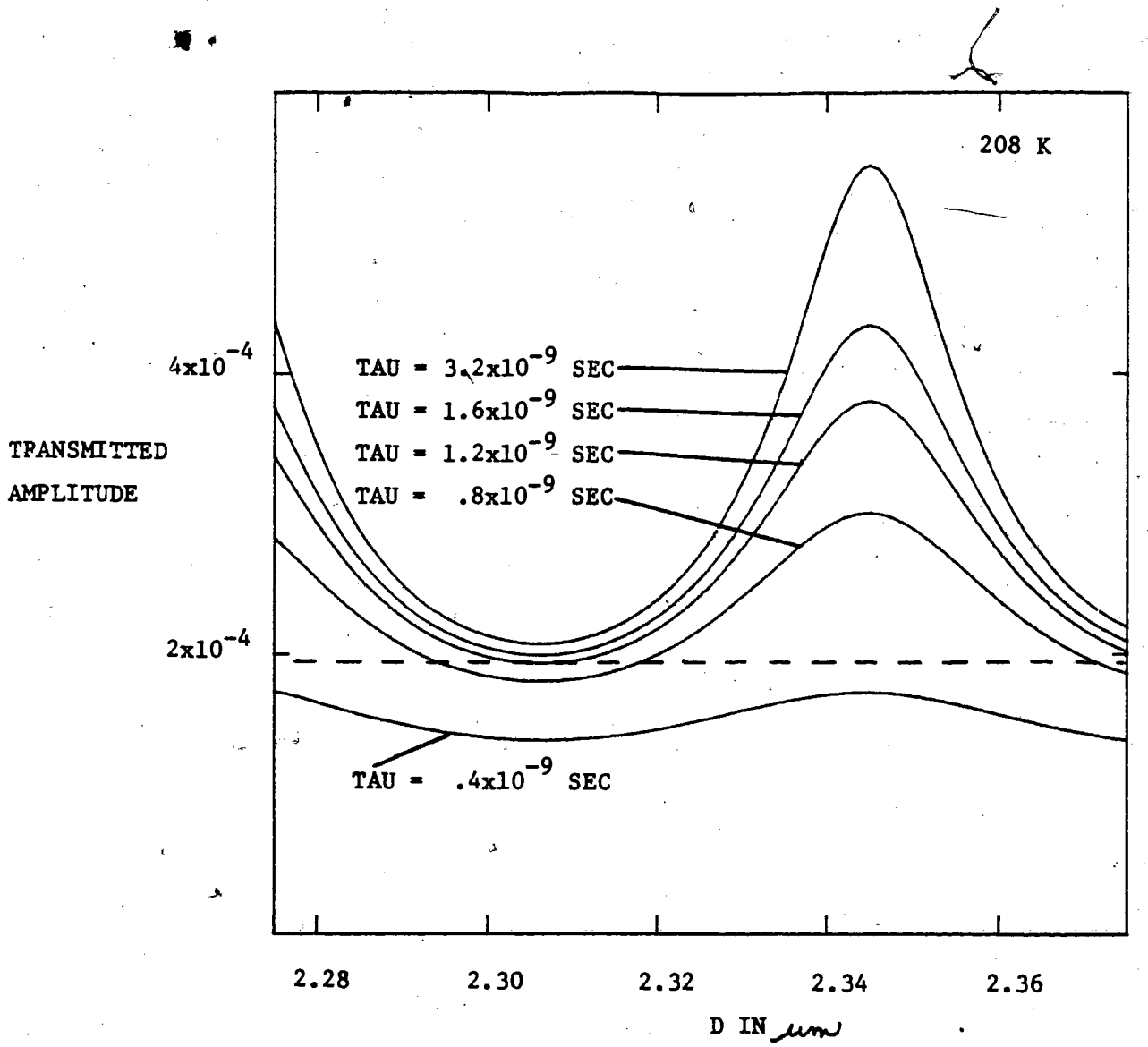

Fig. 4.6 The transmitted amplitude at FMR as a function of sample thickness for various values of tau. The dashed line shows the experimentally observed signal strength and the solid lines were calculated using R=4.302 μohm-cm, F=23.943 GHz, ω/γ =7.822 KOe, $4\pi M_s$=6.392 KOe, $2K_1/M_s$=-770 Oe, H_o=5.99 KOe, A=1 x 10^{-6} ergs/cm, B_2=1.30 x 10^8 ergs/cm^3, density=8.935 g/cm^3, G=3.15 x 10^8 Hz and C_{44}=1.268 x 10^{12}.

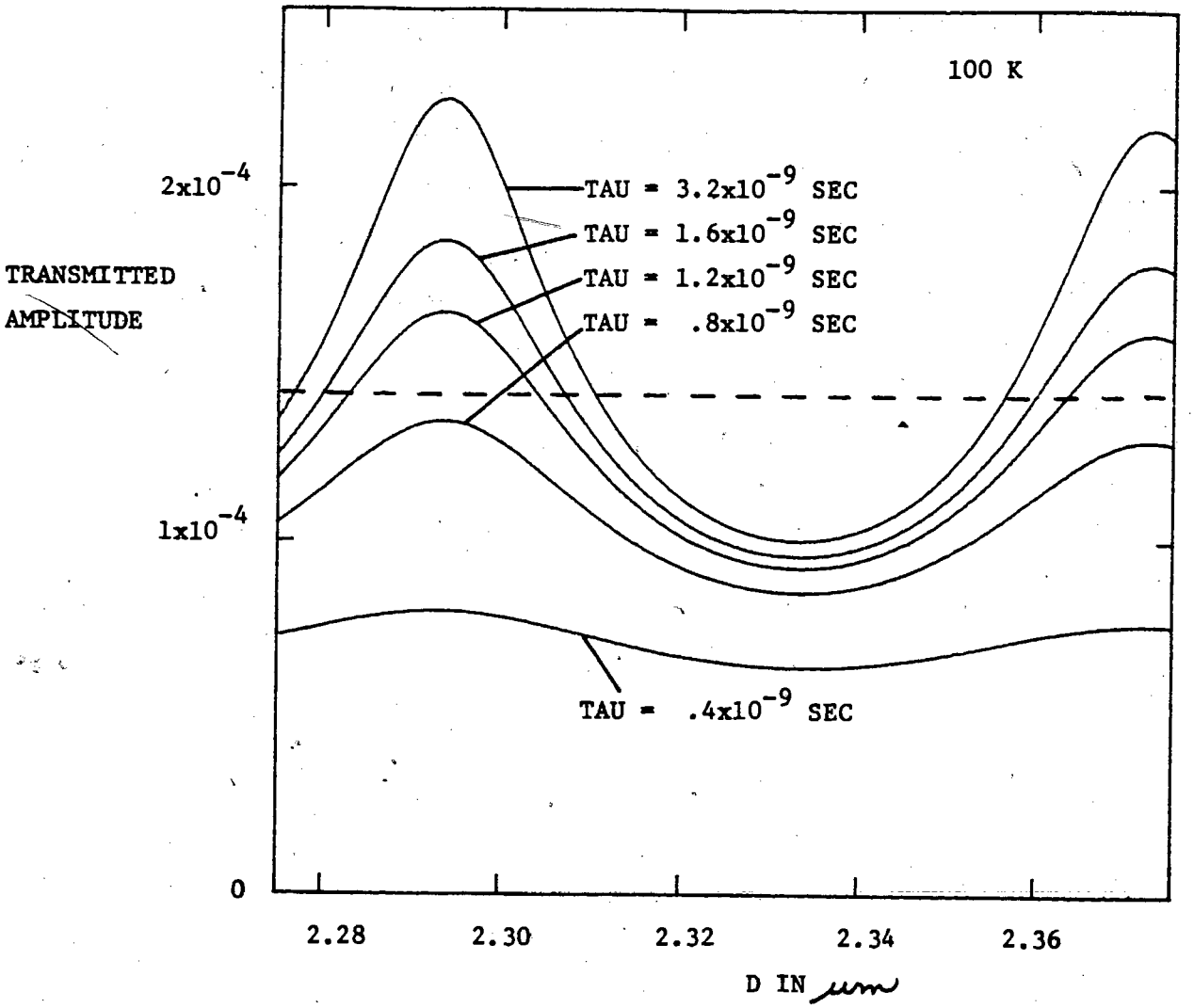

Fig. 4.7 The transmitted amplitude at FMR as a function of sample thickness for various values of tau. The dashed line shows the experimentally observed signal strength and the solid lines were calculated using $R=1.275\ \mu$ohm-cm, $F=23.943$ GHz, $\omega/\gamma=7.822$ KOe, $4\pi M_s=6.548$ KOe, $2K_1/M_s=2000$ Oe, $H_o=7.50$ KOe, $A=1 \times 10^{-6}$ ergs/cm, $B_2=1.48 \times 10^8$ ergs/cm^3, density=8.962 g/cm^3, $G=5.10 \times 10^8$ Hz and $C_{44}=1.301 \times 10^{12}$.

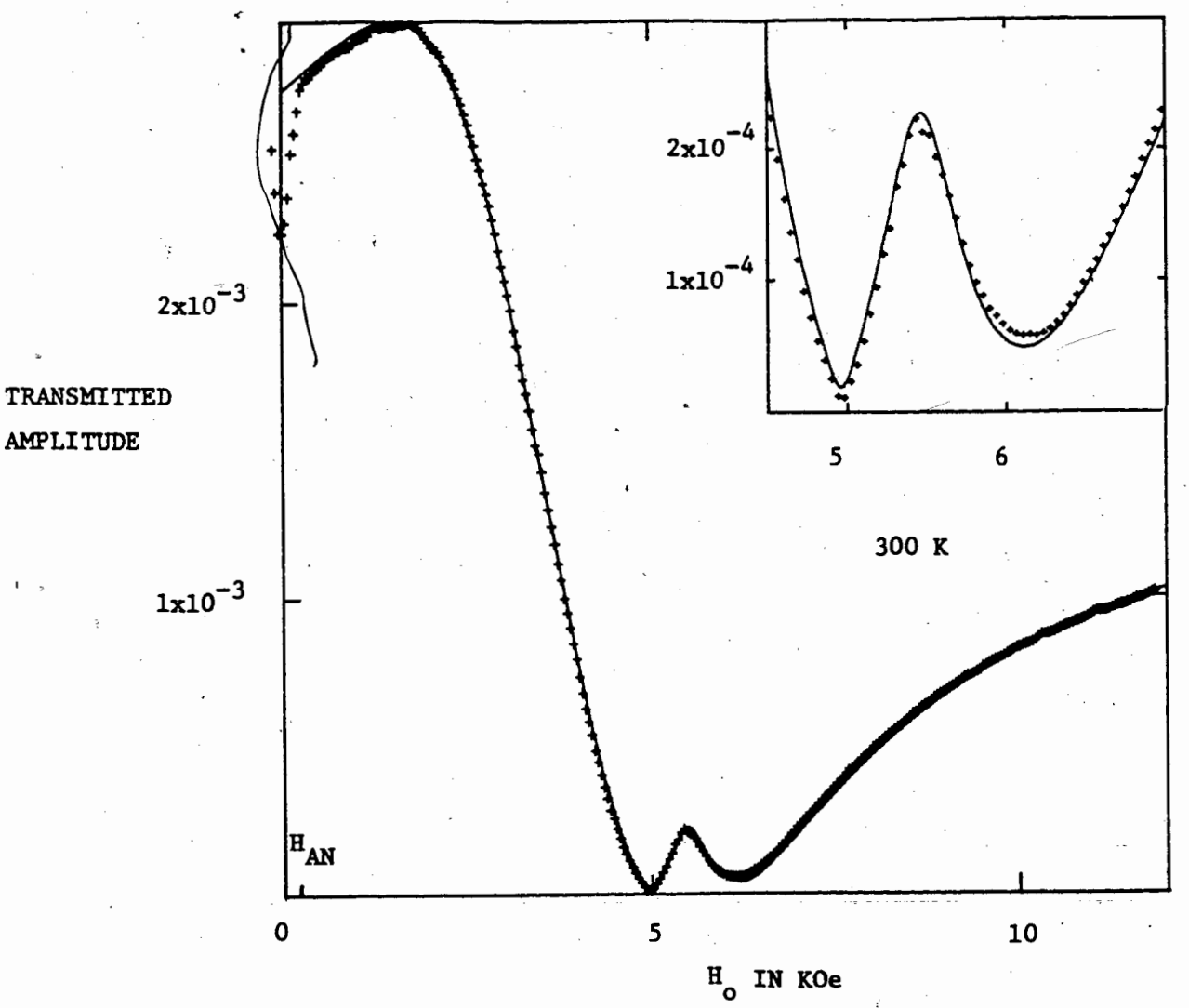

Fig. 4.8 The transmission amplitude as a function of the applied field. The crosses (+) represent experimental data and the solid line was calculated using R=7.529 μ ohm-cm, F=23.943 GHz, ω/γ =7.822 KOe, $4\pi M_s$=6.143 KOe, $2K_1/M_s$=-240 Oe, D=2.310 μm, A=1 x 10^{-6} ergs/cm, B_2=1.07 x 10^8 ergs/cm^3, density=8.9055 g/cm^3, C_{44}=1.234 x 10^{12}, tau=.9 x 10^{-9} and G=3.0 x 10^8 Hz in the field region from 5-6.5 KOe for all other fields a magnetic damping of G=2.45 x 10^8 Hz was used. The inset shows the quality of the fit in the region of FMR.

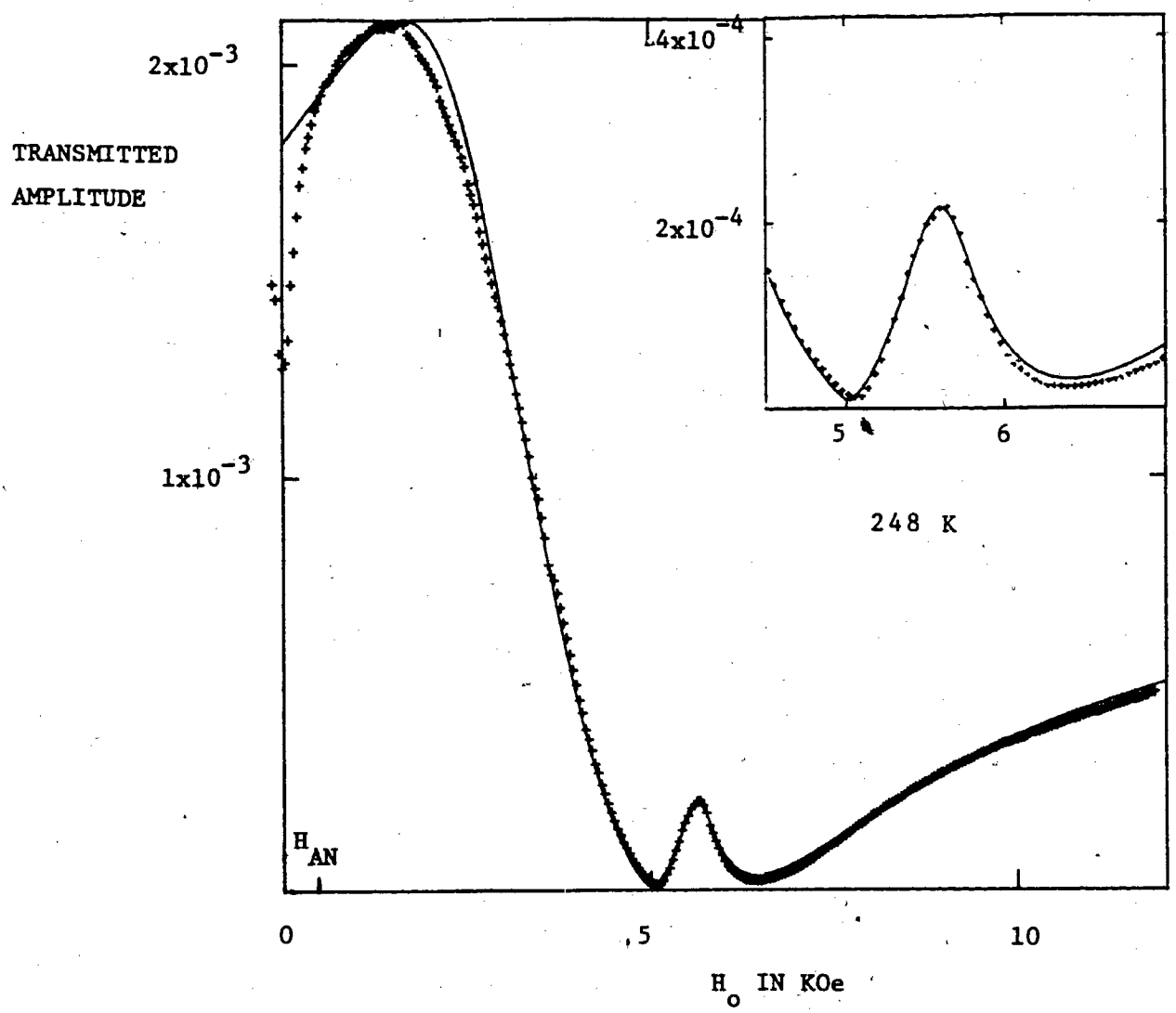

Fig. 4.9 The transmission amplitude as a function of the applied field. The crosses (+) represent experimental data and the solid line was calculated using R=5.606 μ ohm-cm, F=23.943 GHz, ω/γ =7.822 KOe, $4\pi M_s$=6.290 KOe, $2K_1/M_s$=-435 Oe, D=2.308 μm, A=1 x 10^{-6} ergs/cm, B_2=1.21 x 10^8 ergs/cm^3, density=8.923 g/cm^3, C_{44}=1.247 x 10^{12}, tau=.9 x 10^{-9}. and G=3.0 x 10^8 Hz in the field region from 5-6.5 KOe. For all other fields a magnetic damping of G=2.45 x 10^8 Hz was used. The inset shows the quality of the fit in the region of FMR.

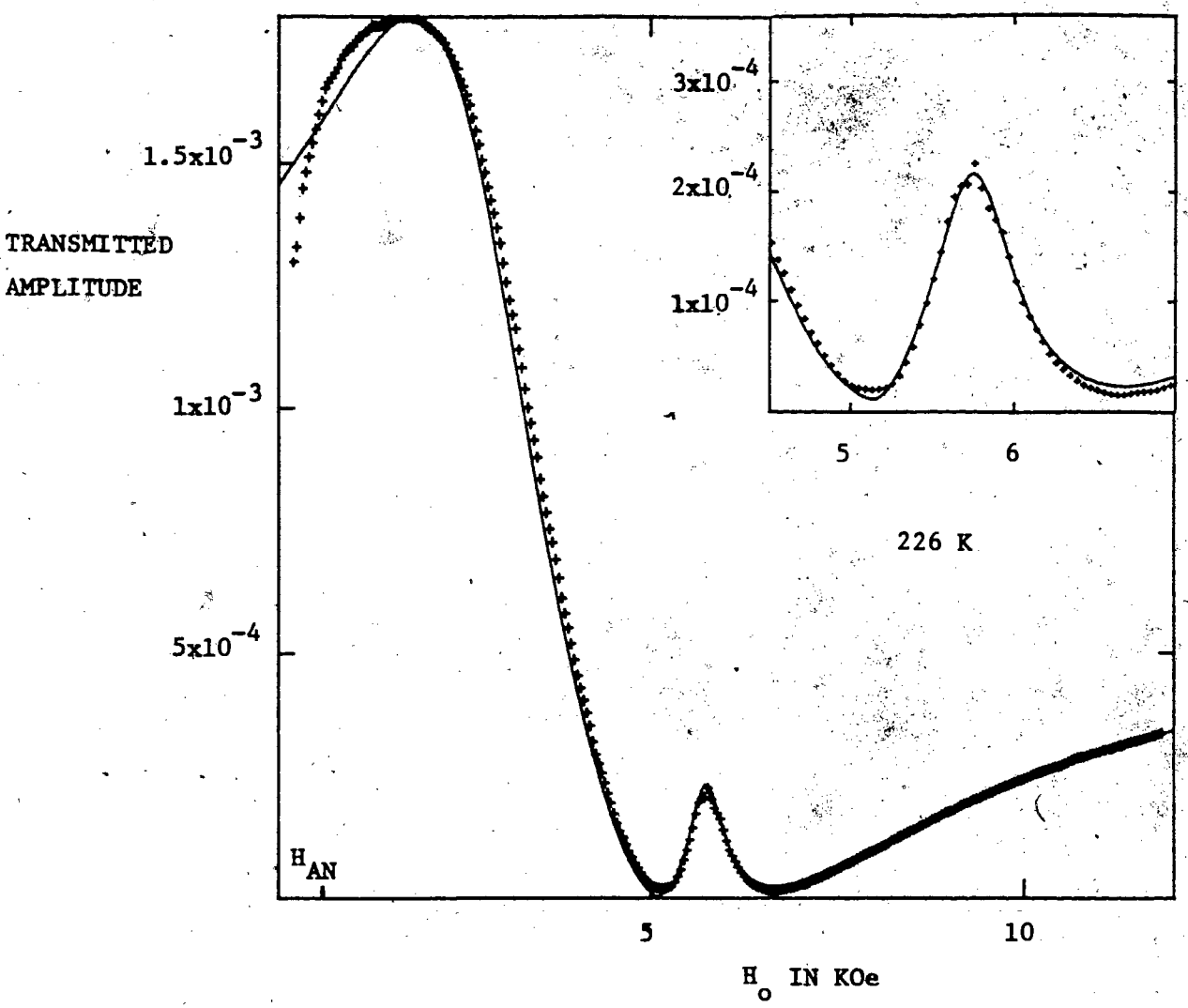

Fig. 4.10 The transmission amplitude as a function of the applied field. The crosses (+) represent experimental data and the solid line was calculated using R=4.890 μ ohm-cm, F=23.943 GHz, ω/γ =7.822 KOe, $4\pi M_s$=6.354 KOe, $2K_1/M_s$=-630 Oe, D=2.307 μm, A=1 x 10^{-6} ergs/cm, B_2=1.26 x 10^8 ergs/cm^3, density=8.929 g/cm^3, C_{44}=1.255 x 10^{12}, tau=1.1 x 10^{-9}, and G=3.0 x 10^8 Hz in the field region from 5-6.5 KOe. For all other fields a magnetic damping of G=2.45 x 10^8 Hz was used. The inset shows the quality of the fit in the region of FMR.

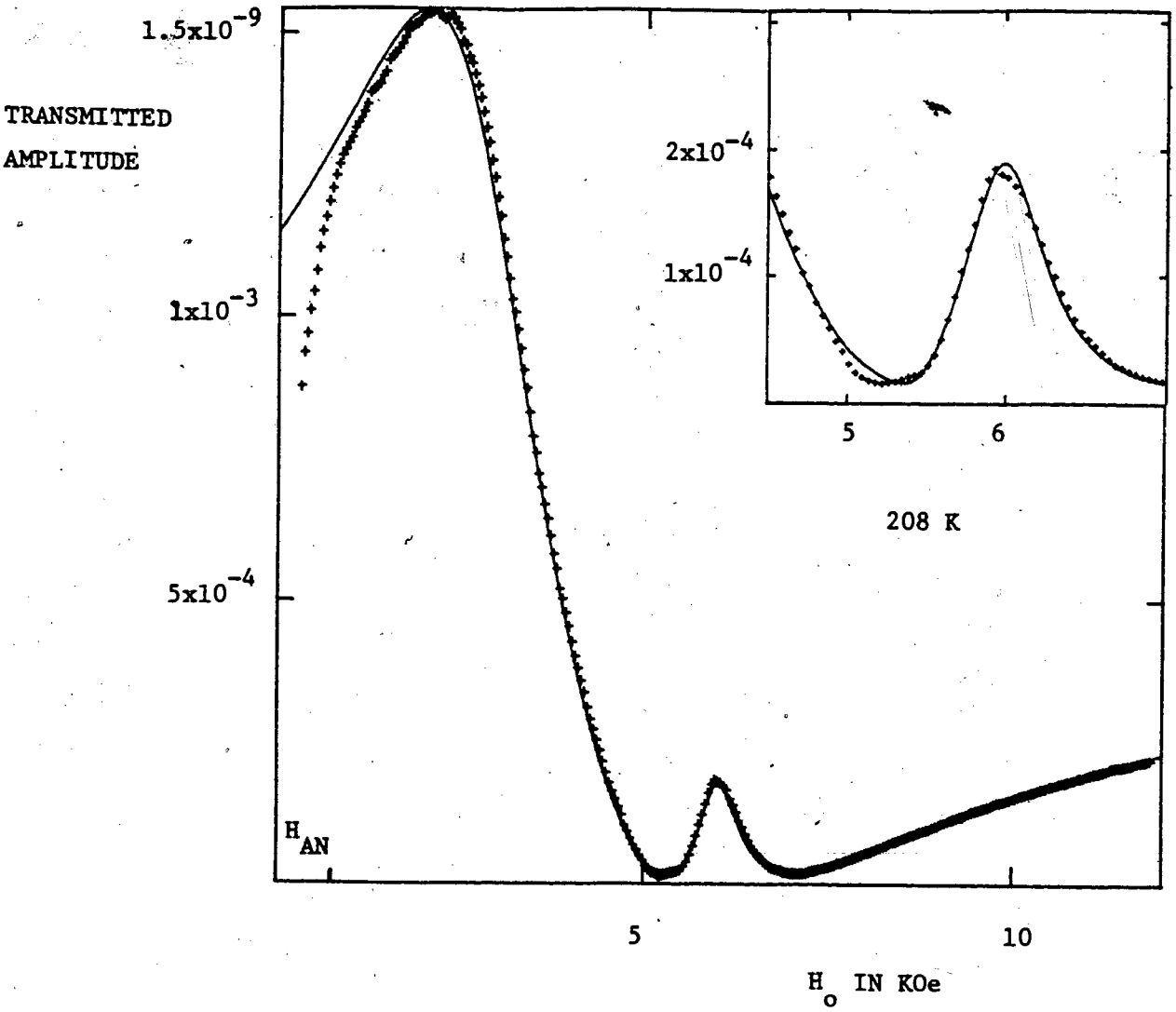

Fig. 4.11 The transmission amplitude as a function of the applied field. The crosses (+) represent experimental data and the solid line was calculated using R=4.302 μ ohm-cm, F=23.943 GHz, ω/γ =7.822 KOe, $4\pi M_s$=6.398 KOe, $2K_1/M_s$=-770 Oe, D=2.307 μm, A=1 x 10^{-6} ergs/cm, B_2=1.30 x 10^8 ergs/cm^3, density=8.935 g/cm^3, C_{44}=1.268 x 10^{12}, tau=1.2 x 10^{-9}, and G=3.15 x 10^8 Hz in the field region from 5-6.5 KOe. For all other fields a magnetic damping of G=2.45 x 10^8 Hz was used. The inset shows the quality of the fit in the region of FMR.

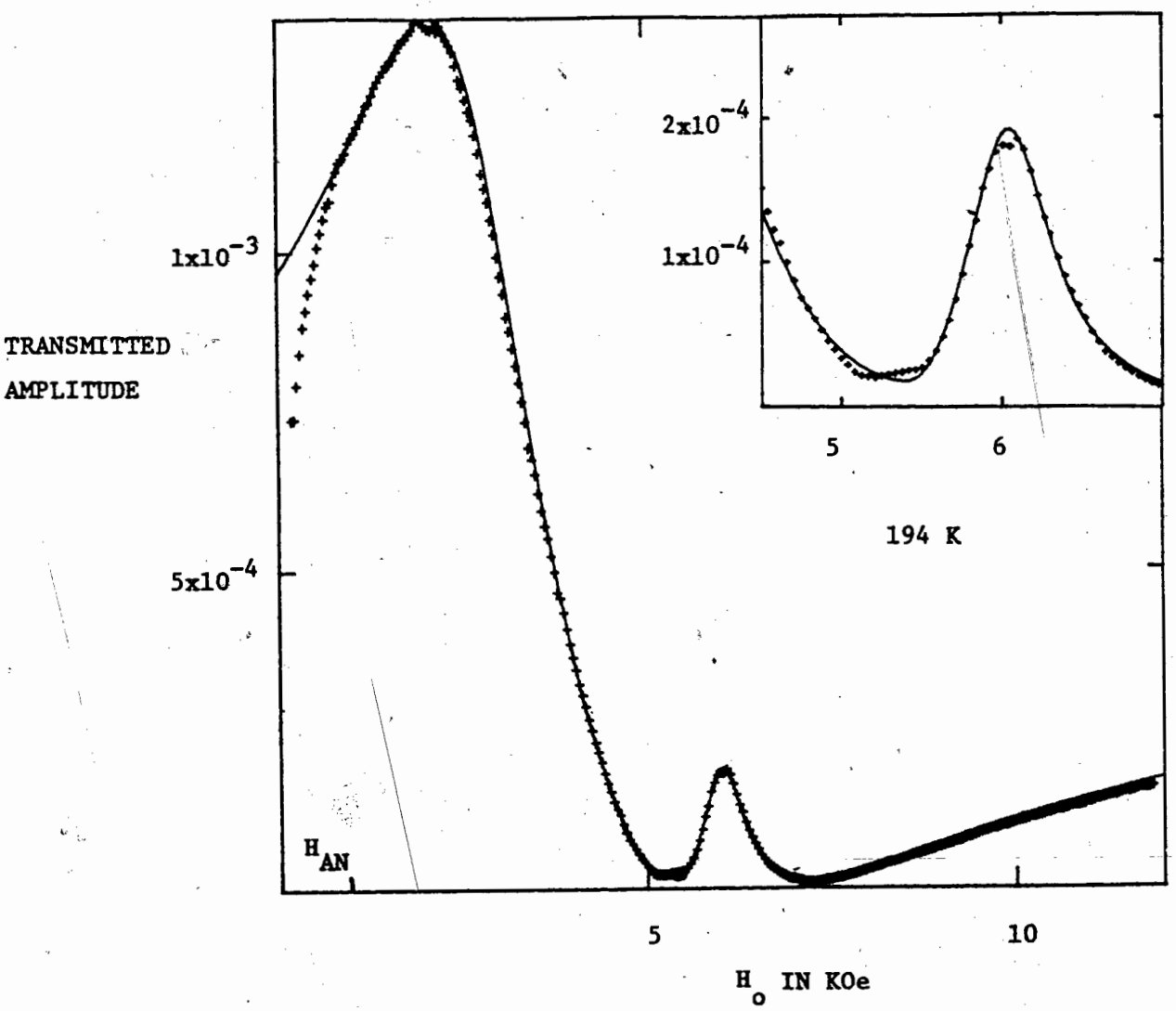

Fig. 4.12 The transmission amplitude as a function of the applied field. The crosses (+) represent experimental data and the solid line was calculated using R=3.854 μ ohm-cm, F=23.943 GHz, ω/γ =7.822 KOe, $4\pi M_s$=6.420 KOe, $2K_1/M_s$=-950 Oe, D=2.307 μm, A=1 x 10^{-6} ergs/cm, B_2=1.33 x 10^8 ergs/cm^3, density=8.939 g/cm^3, C_{44}=1.273 x 10^{12}, tau=1.0 x 10^{-9}, and G=3.2 x 10^8 Hz in the field region from 5-6.5 KOe. For all other fields a magnetic damping of G=2.45 x 10^8 Hz was used. The inset shows the quality of the fit in the region of FMR.

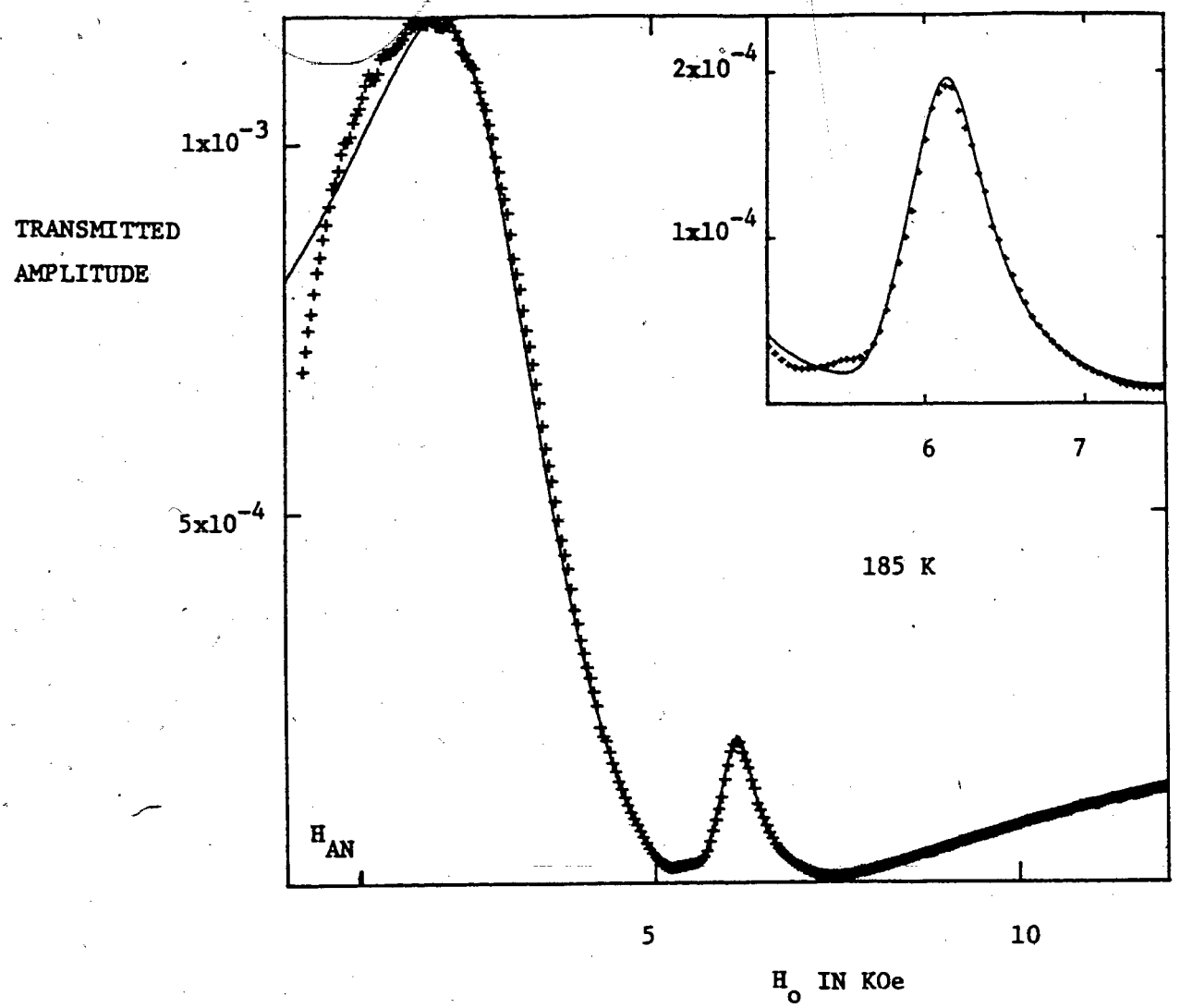

Fig. 4.13 The transmission amplitude as a function of the applied field. The crosses (+) represent experimental data and the solid line was calculated using R=3.572 μ ohm-cm, F=23.943 GHz, ω/γ =7.822 KOe, $4\pi M_s$=6.436 KOe, $2K_1/M_s$=-1070 Oe, D=2.306 μm, A=1 x 10^{-6} ergs/cm, B_2=1.35 x 10^8 ergs/cm^3, density=8.942 g/cm^3, C_{44}=1.276 x 10^{12}, tau=1.0 x 10^{-9}, and G=3.2 x 10^8 Hz in the field region from 5-6.5 KOe. For all other fields a magnetic damping of G=2.45 x 10^8 Hz was used. The inset shows the quality of the fit in the region of FMR.

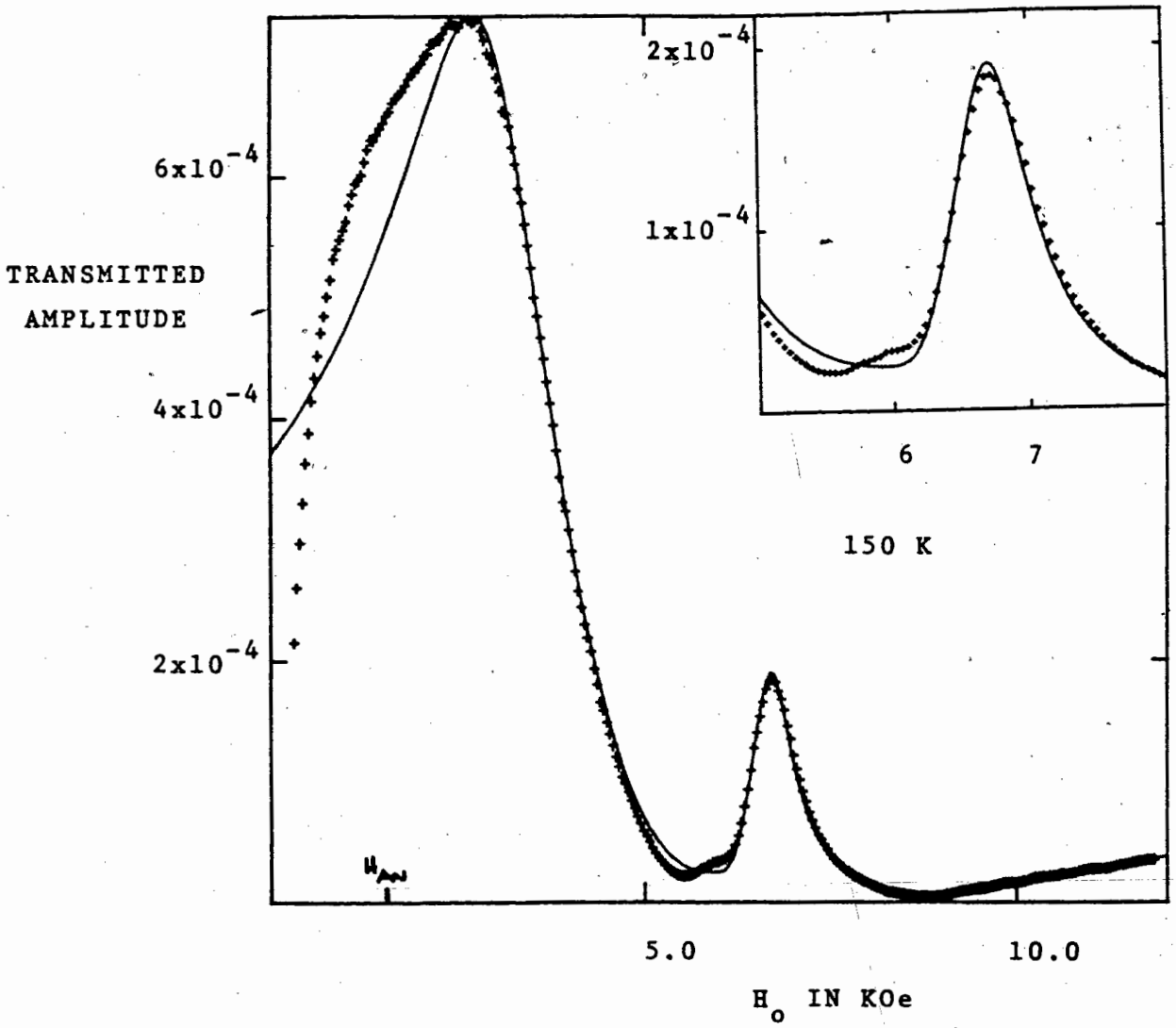

Fig. 4.14 The transmission amplitude as a function of the applied field. The crosses (+) represent experimental data and the solid line was calculated using R=2.533 μ ohm-cm, F=23.943 GHz, ω/γ =7.822 KOe, $4\pi M_s$=6.490 KOe, $2K_1/M_s$=-1640 Oe, D=2.305 μm, A=1 x 10^{-6} ergs/cm, B_2=1.41 x 10^8 ergs/cm^3, density=8.951 g/cm^3, C_{44}=1.288 x 10^{12}, tau=1.3 x 10^{-9}, and G=3.7 x 10^8 Hz in the field region from 6-8.5 KOe. For all other fields a magnetic damping of G=3.10 x 10^8 Hz was used. The inset shows the quality of the fit in the region of FMR.

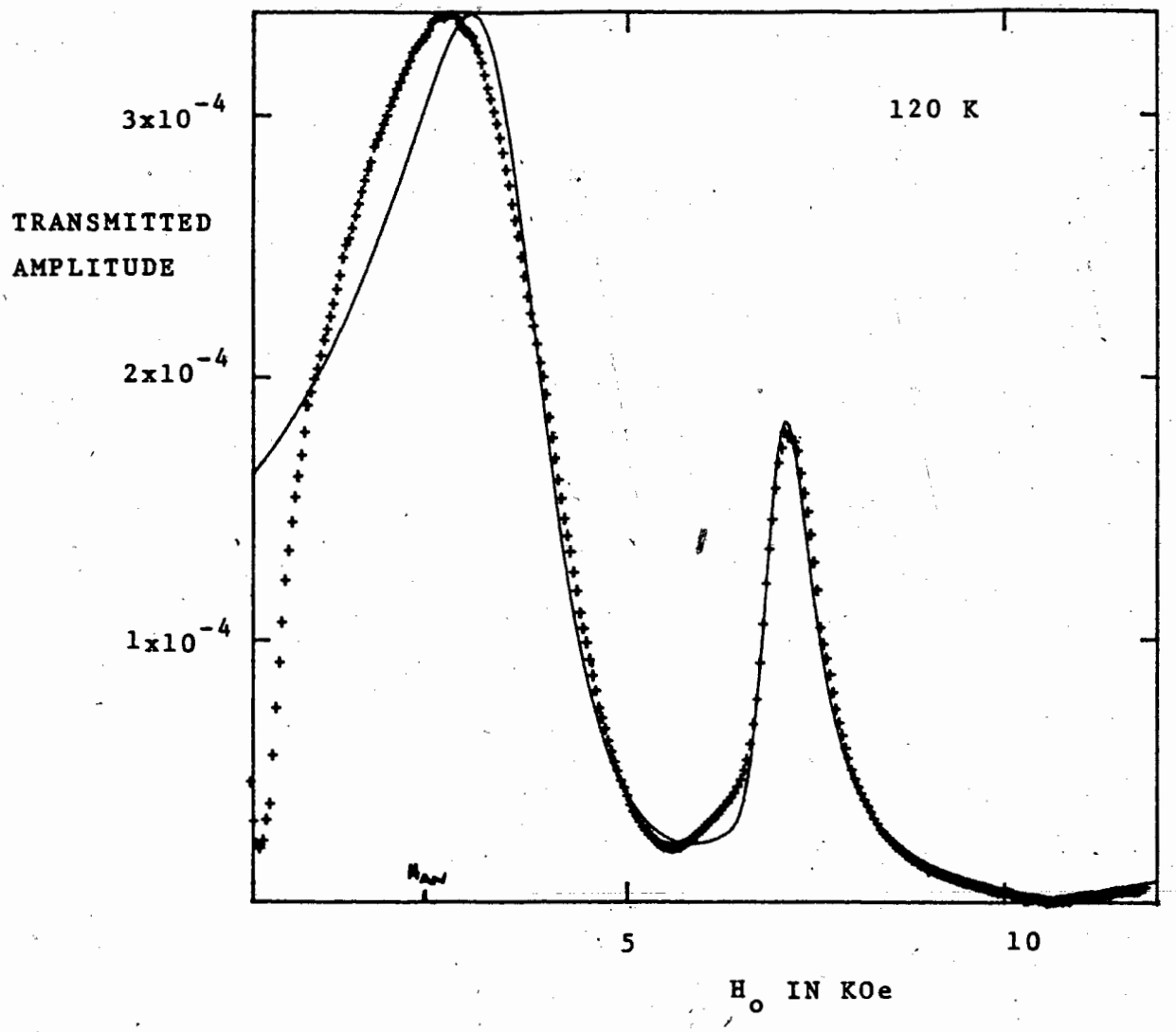

Fig. 4.15 The transmission amplitude as a function of the applied field. The crosses (+) represent experimental data and the solid line was calculated using R=1.869 μ ohm-cm, F=23.943 GHz, ω/γ =7.822 KOe, $4\pi M_s$=6.522 KOe, $2K_1/M_s$=-2300 Oe, D=2.305 μm, A=1 x 10^{-6} ergs/cm, B_2=1.45 x 10^8 ergs/cm^3, density=8.957 g/cm^3, C_{44}=1.298 x 10^{12}, tau=1.4 x 10^{-9}, and G=4.3 x 10^8 Hz in the field region above 6 KOe and a magnetic damping of G=5.3 x 10^8 Hz was used at fields below 6 KOe.

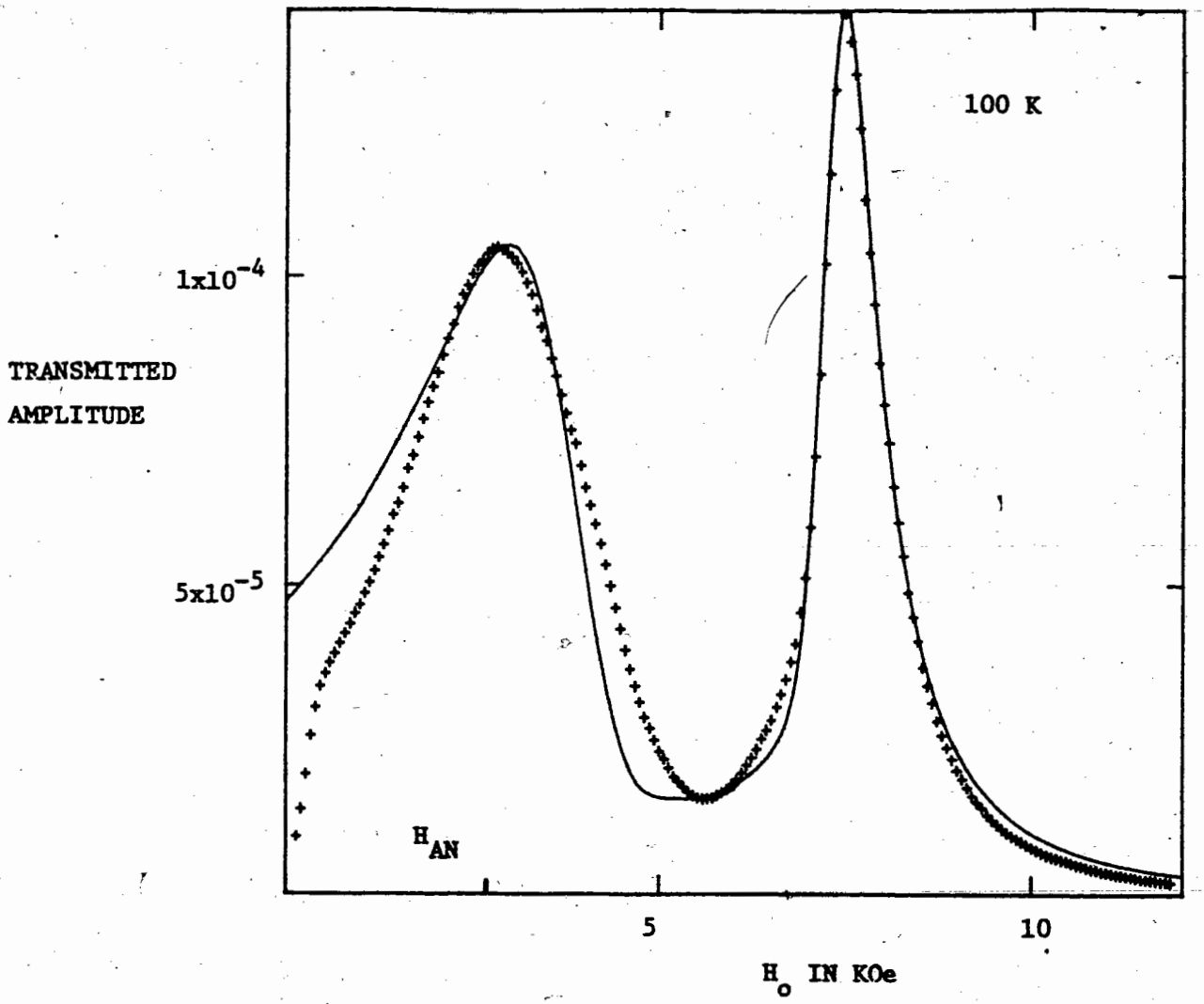

Fig. 4.16 The transmission amplitude as a function of the applied field. The crosses (+) represent experimental data and the solid line was calculated using R=1.275 μ ohm-cm, F=23.943 GHz, ω/γ =7.822 KOe, $4\pi M_s$=6.548 KOe, $2K_1/M_s$=-2750 Oe, D=2.305 μm, A=1 x 10^{-6} ergs/cm, B_2=1.48 x 10^8 ergs/cm^3, density=8.962 g/cm^3, C_{44}=1.301 x 10^{12}, tau=1.3 x 10^{-9}, and G=5.1 x 10^8 Hz in the field region above 6 KOe and a magnetic damping of G=8.3 x 10^8 Hz was used for fields below 6 KOe.

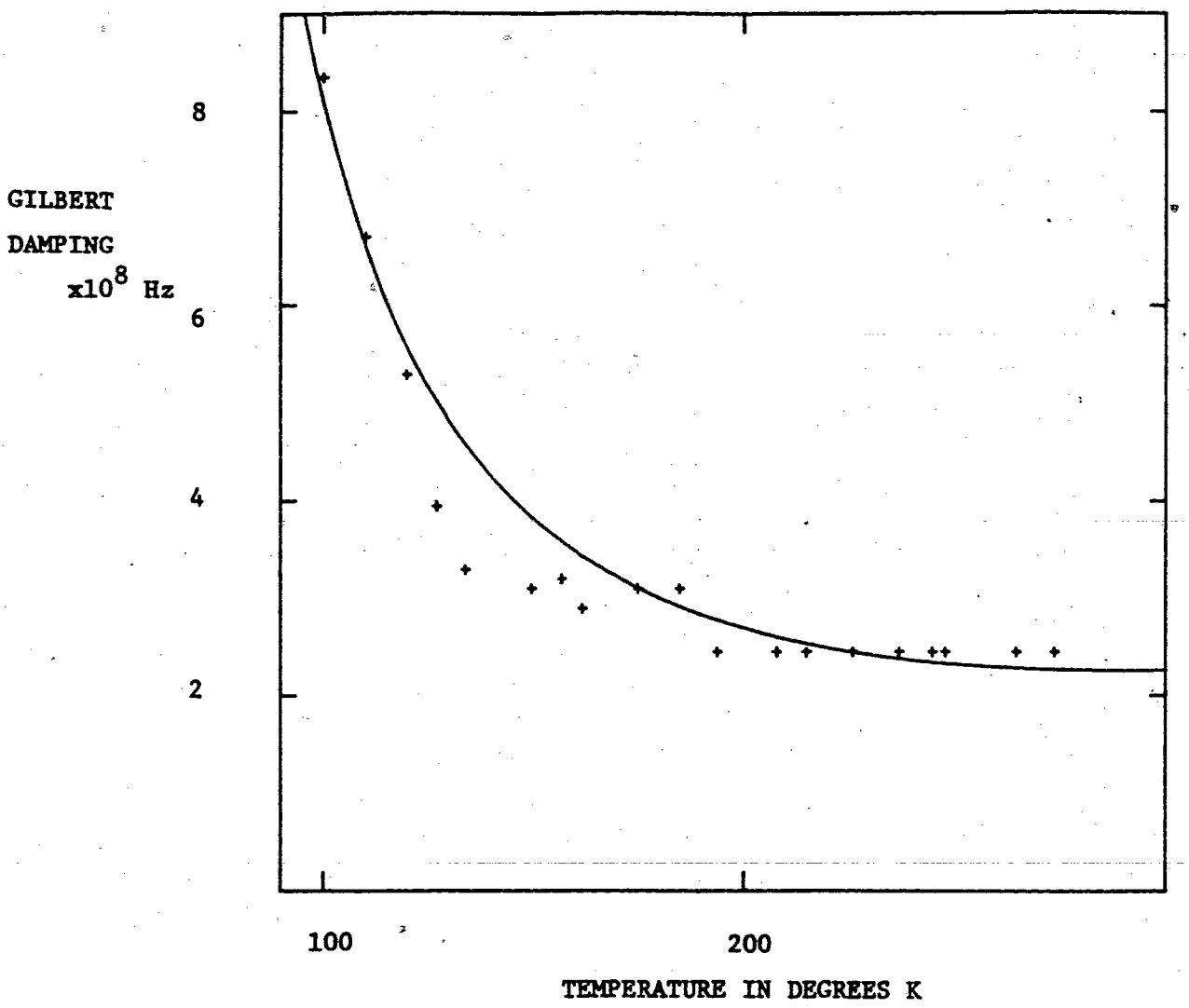

Fig. 4.17 The temperature dependence of the magnetic damping parameter measured at FMAR. The solid curve shows the results of Heinrich, Meredith and Cochran.

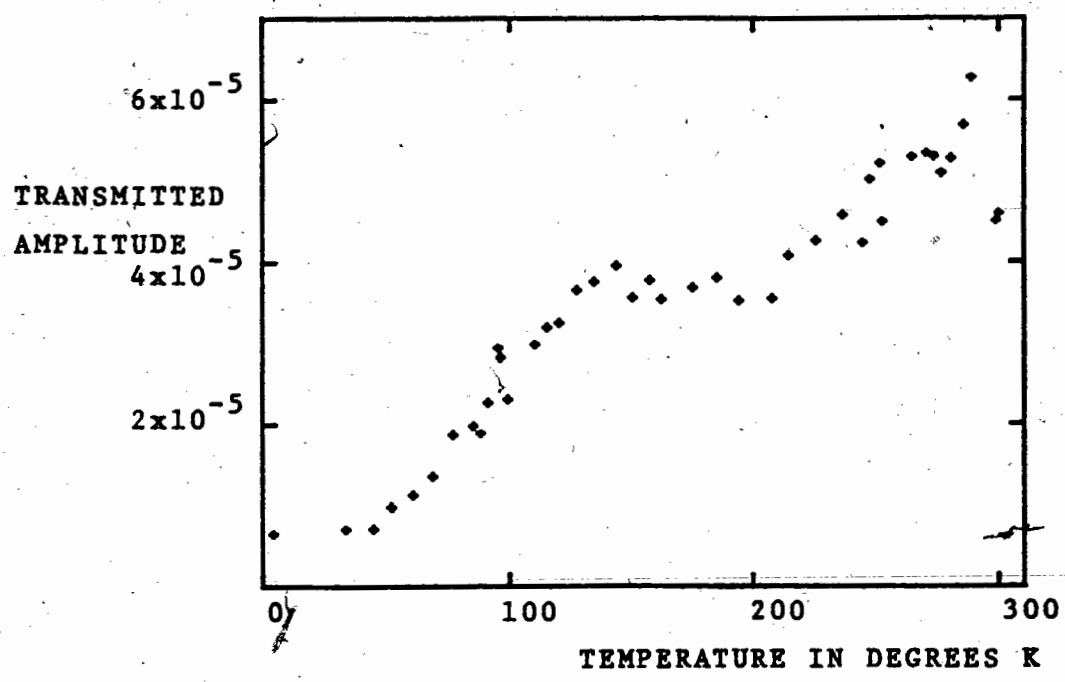

Fig. 4.18 The temperature dependence of the transmission amplitude at FMR.

V. DISCUSSION

In general the theory outlined in chapter 2 gave a good fit to the observed transmission signals. The observed temperature dependence of the magnetic damping at FMAR was found to agree to within experimental error with the results obtained by Heinrich et al [1]. In addition a magnetic damping at FMR which was $.7 \times 10^8$ Hz larger than that measured by Bhagat and Lubitz [3], was found to give a good fit to the linewidth of the ultrasonic signal. This additional damping at FMR is probably due to the presence of surface imperfections.

Magnetic Damping

At this point a brief discussion about the origin of magnetic damping in metals is in order. In addition to the damping which results from the presence of imperfections (ie two magnon scattering [8]), there is a large intrinsic damping associated with the presence of the conduction electrons. Hodges, Stone and Gold [35] have shown that the shape of the Fermi surface changes when the direction of the sample magnetization is changed. Hence the Fermi surface will be continually changing shape in response to a precessing magnetization and the distribution of the electrons will always lag behind the instantaneous equilibrium distribution. This phase lag gives rise to a magnetic damping term. If the electron relaxation time is much shorter than the period of precession we find that the magnetic damping from this source is proportional to the relaxation time τ (or the DC conductivity σ). This damping mechanism was proposed by Kambersky [5] and was later extended by Korenmann and Prange [6] who made an estimate of

the size of the magnetic damping based on a band theory model of ferromagnetism in which spin orbit coupling had been included. Korenmann and Prange found that the magnetic damping was approximately proportional to the wavenumber dependent electrical conductivity

$$G \propto \sigma \frac{\text{TAN}^{-1} KL}{KL}$$

where $L = V_F \tau$ is the electron mean free path and K is the wavenumber associated with the magnetic disturbance.

Another source of magnetic damping arises from the finite spin lifetime of the ferromagnetic electrons. A number of authors have studied this problem [36,37,38] and found that in our temperature range the magnetic damping should be proportional to $1/\tau$ (or the DC resistivity ρ) where τ is the conduction electron relaxation time.

As a result of these considerations Heinrich et al [1] made a fit to the magnetic damping measured at FMAR using two terms, one proportional to σ (at FMAR $KL<1$ and so $(\tan^{-1}KL)/KL=1$) and one proportional to ρ . They obtained a good fit to the observed damping using the formula

$$G = 1.07 \times 10^8 \sigma(T)/\sigma_{(300)} + 1.19 \times 10^8 \rho(t)/\rho_{(300)}$$

This formula was used to draw the solid line shown in Fig. (4.17) and is in agreement with the results we have obtained to within the uncertainty of the experiment.

Ultrasonic Attenuation

There are a number of mechanisms which give rise to ultrasonic attenuation in a ferromagnetic metal. One of the largest of these results from the magnetoelastic coupling between the lattice and the magnetization. This term was included in the theory outlined in chapter 2 and gives rise to the magnetic field dependent ultrasonic attenuation which is shown in Fig. 2.10. This contribution results in an ultrasonic energy decay length of $\approx 5\mu m$ (a lifetime of 1.5×10^{-9} sec) at FMR at room temperature: (It should be noted that this attenuation occurs in addition to the damping related to the value of tau.)

The finite ultrasonic energy decay time tau accounts for the ultrasonic attenuation caused by the following mechanisms. The first of which results from interactions between the ultrasonic wave and the conduction electrons. This effect has been studied in considerable detail since the measurement of ultrasonic attenuation in superconducting materials provides usefull information about the size of the energy gap (see [39,40]). In normal metals energy is lost from the acoustic wave because the motion of the conduction electrons lags slightly behind that of the lattice. The motion of the electrons relative to the lattice gives rise to an ohmic loss. The calculation of the rate of attenuation is complicated by the fact that at low temperatures the electron mean free path becomes longer than the acoustic wavelength. This problem has been addressed by a number of authors (Pippard [41], Steinberg [42], Cohen, Harrison and Harrison [43] and Banic and Overhauser [44]). The attenuation length reaches a minimum at helium temperatures and by using equation 3.5 of Steinberg [42] with the modification that we include the permeability μ in the calculation of the skin depth ($K_0^2 = 1/\delta^2$ becomes $K_0^2 = \frac{4\pi\omega\sigma\mu}{c^2}$)

we find that the attenuation length from this source is at worst 60 μm (a lifetime of more than 20 nsec.) and so it is unlikely that the conduction electrons produce a significant amount of ultrasonic signal attenuation in our samples.

A third source of energy loss results from the coupling of the ultrasonic wave to thermal phonons by means of anharmonic terms in the stress strain tensor. The presence of anharmonic terms causes the equilibrium conditions for the thermal phonons to vary with time when an ultrasonic wave is present. The phonons will continually relax back toward thermal equilibrium and in doing so will damp the ultrasonic signal. This source of damping was first pointed out by Akhieser [45] and has since been treated theoretically by Bommel and Dransfeld [46], Woodruff and Ehrenrich [47] and Mason and Bateman [48]. This is the dominant loss mechanism in many insulating crystals at room temperature. Oliver and Slack [49] present an approximate expression for the room temperature sound attenuation which was based on the results of Woodruff and Ehrenreich. This expression yields an ultrasonic relaxation time of approximately 1 nsec. This relaxation time is expected to be only weakly temperature dependent for sample temperatures larger than $\approx .2\,\Theta_{Debye}$ (75 K for Ni).

We have also observed that there was a marked decrease in the size of the signal transmitted at FMR after the sample had been mechanically deformed. This suggests that dislocations play a role in determining the attenuation length. Granato and Lucke [50] have studied the attenuation of sound by dislocations . The observed rise in the ultrasonic attenuation could be accounted for with a reasonable dislocation density ($N \approx 10^{10}/cm^2$).

Summary

Perhaps the most useful result of this work was the development of a technique for producing thin single crystals of uniform thickness. These crystals can be grown to thicknesses in excess of 20 μm and appear to have material properties which are indistinguishable from bulk nickel. In the unannealed state the epitaxially grown crystals have a higher residual restivity ratio (RRR > 200) than is found in nickel crystals grown by the Czochralski technique (RRR 70). This work confirms the earlier measurements of the temperature dependence of the magnetic damping at FMAR made by Heinrich, Meredith and Cochran [1]. The large ultrasonic signal centered at FMR prevented us from determining the magnetic damping at temperatures below 100 K.

The observed ultrasonic signal amplitude could be accounted for by using the bulk value of the magnetostriction constant, and by using an ultrasonic energy decay time of 1.2 nsec (a mean free path of $\approx 5 \mu m$). This is believed to be the first measurement of the ultrasonic mean free path in nickel at a frequency above 9 GHz. The observed ultrasonic attenuation can be accounted for by two effects: the absorption of sound by dislocations and the attenuation due to coupling of the ultrasonic wave to thermal phonons by anharmonic terms in the stress strain tensor.

In order to extend the measurement of the magnetic damping at FMAR to lower temperatures it appears that we must produce samples with a non-uniform thickness. This could be done either modifying the plating cell geometry so as to produce wedge shaped samples or by electropolishing the samples after they had been grown (electropolishing produces a slightly rippled surface). A more accurate determination of the temperature dependence of the ultrasonic attenuation could be made if thicker samples

were used. The use of thicker samples would also reduce the size of the acoustic standing waves which made the knowledge of the exact sample thickness a crucial factor in the determination of the temperature dependence of the ultrasonic attenuation.

It is also possible to determine the exchange constant by measuring the separation between FMR and the peak in the magnetoelastic component of the ultrasonic attenuation. This separation was too large to be readily measured at 24 GHz, however, as the separation is proportional to the frequency squared measurements made at lower frequencies can be used to determine the exchange constant. Reference [18] contains our preliminary results of the ultrasonic determination of exchange at 9.5 GHz.

Bibliography

1. B. Heinrich, D.J. Meredith and J.F. Cochran, J. Appl Phys. 50, 7726 (1979).
2. S.M. Bhagat and L.L. Hirst, Phys. Rev. 151, 401 (1966).
3. S.M. Bhagat and P. Lubitz, Phys. Rev. B10, 179 (1974).
4. J.N. Lloyd and S.M. Bhagat, Sol. St. Comm. 8, 2029 (1970).
5. V. Kambersky, Can. J. Phys. 48, 2906 (1970).
6. V. Korenmann and R.E. Prange, Phys. Rev. B6, 2769 (1972).
7. T.L. Gilbrt, Phys. Rev. 100, 1234 (1955).
8. Marshall Sparks, "Ferromagnetic Relaxation Theory", McGraw-Hill, N.Y., (1964).
9. B. Heinrich and V. Meshcheryakov, JETP Lett. 9, 378 (1969).
10. B. Heinrich and V. Meshcheryakov, Sov. Phys. JETP 32 232 (1971).
11. J.G. Wright, Thin Solid Films 9, 309 (1972).
12. B. Heinrich and J.F. Cochran, J. Appl. Phys. 50, 2440 (1979).
13. S. Chikazumi, "Physics of Magnetism" John Wiley And Sons Inc., N.Y., (1964).
14. L. Kraus and Z. Frait, Czech. J. Phys. B23, 188 (1973).
15. J.R. Macdonald, Proc. Phys. Soc. London A 64, 968 (1951).
16. J.F. Cochran, B. Heinrich and G. Dewar, Can. J. Phys. 55, 834 (1977).
17. G.T. Rado and J.R. Weertman, J. Phys. Chem. Solids 11, 315 (1959).
18. B. Heinrich, J.F. Cochran and K. Myrtle, J. Appl. Phys. 53, 2092 (1982).
19. W.J. McG. Tegart, "The Electrolytic and chemical Polishing of Metals" Pergamon Press, London, (1959).
20. J.G. Wright, Section 2.3 in Epitaxial Growth Part A, Academic Press, N.Y. (1975) J.W. Matthews Ed.
21. J. Goddard and J.G. Wright, Brit. J. Appl. Phys. 15, 807 (1964).
22. M.R. Chodkowski and R. Weil, J. Electrochem. Soc. 124, 1678 (1977).
23. U. Bertocci and C. Bertocci, J. Electrochem. Soc. 118, 1287 (1971).
24. Americian Institute of Physics Handbook, 3rd ed., McGraw-Hill N.Y., (1972).
25. R. Weil and H.J. Read, J. Appl. Phys. 21, 1068 (1950).
26. M.J. Laubitz, T. Matsumura and P.J. Kelly, Can. J. Phys. 54, 92 (1976).
27. F.C. Schwerer and J. Silcox, Phys. Rev. Letters 20, 101 (1968).

28. G.K. White and S.B. Woods, Phil. Trans. Roy. Soc. (London) A251, 273 (1959).

29. F.C. Nix and D. MacNair, Phys. Rev. 60, 597 (1941).

30. G.A. Alers, J.R. Neighbours and H. Sato, J. Phys. Chem. Solids 13, 40 (1960).

31. T. Tokunaga, J. Science Hiroshima Univ. Series A 38, 215 (1974).

32. R. Kaul and E.D. Thompson, J. Appl. Phys. 40, 1383 (1969).

33. H. Danan, A. Herr and J.P. Meyer, J. Appl. Phys. 39, 669 (1968).

34. E.W. Lee and M.A. Asgar, Proc. Roy. Soc. (London) A326, 73 (1971).

35. L. Hodges, D.R. Stone and A.V. Gold, Phys. Rev. Letters, 19, 655 (1967).

36. R.J. Elliott, Phys. Rev. 96, 266 (1954).

37. B. Heinrich, D. Fraitova and V. Kambersky, Phys. Stat. Sol. 23, 501 (1967).

38. V. Kambersky, Czech J. Phys. B26, 1366 (1976).

39. R.T. Beyer and S.V. Letcher, "Physical Ultrasonics" Academic Press, N.Y., (1969).

40. J.W. Tucker and V.W. Rampton, "Microwave Ultrasonics in Solid State Physics" North-Holland Publishing Co., Amsterdam, (1972).

41. A.B. Pippard, Phil. Mag. 46, 1104 (1955).

42. M.S. Steinberg, Phys. Rev. 111, 425 (1958).

43. M.H. Cohen, M.J. Harrison and W.A. Harrison, Phys. Rev. 117, 937 (1960).

44. N.C. Banic and A.W. Overhauser, Phys. Rev. B16, 3379 (1977).

45. A. Akhieser, J. Phys. (USSR) 1, 277 (1939).

46. H.E. Bommel and K. Dransfeld, Phys. Rev. 117, 1245 (1960).

47. T.O. Woodruff and H. Ehrenreich, Phys. Rev. 123, 1553 (1961).

48. W.P. Mason and T.B. Bateman, J. Acoust. Soc. Am. 36, 644 (1964).

49. D.W. Oliver and G.A. Slack, J. Appl. Phys. 37, 1542 (1966).

50. A.V. Granato and K. Lucke, J. Appl. Phys. 27, 583 (1956).